RSC Advances

REVIEW

View Article Online
View Journal | View Issue

Cite this: *RSC Adv.*, 2026, **16**, 28323

Indian knowledge system plant based carbon dots: synthesis and optical sensing applications for environmental remediation

Inderbir Kaur,[a] Vandana Batra,[b] Jasmina Baveja,[c] J. Mejia,[d] Y. Kumar[de] and V. Agarwal *[d]

One of the major problems in recent decades has been the absorption of harmful chemicals and toxins into the human body, either directly or indirectly. The excessive usage of heavy metals, like Cr(VI), Pb(II), As(II), Cd(II), and organic contaminants such as pesticides, dyes, disinfectants, and food additives, and their untreated discharge by the industries, has had a profound effect on the environmental water systems as well as on the food chain. This ultimately impacts the human race. Carbon dots (CDs), a relatively new, cost-effective and sustainable nanomaterial, has recently gained attention as an alternative solution to address this issue, due to numerous benefits, such as additional value to waste, utilizing pollution-free resources and green processing procedures. Substantial type of precursors for green CDs have employed various plants from Indian knowledge system and have been used to detect metal ions and other organic contaminants in water. Some examples include tulsi leaves for detection of Cr(VI), mango peels for detection of the pesticide, mesotrione, *Aegle marmelos* (bael patra fruit) for detection of allura red, Fe(III), and Cu(II). The CDs synthesised using turmeric powder have been explored for degradation of acid azo dyes. It is well known that the ancient Indian knowledge system has consistently emphasized the role of nature in benefiting the human race. Vast Indian plant wealth is now finding alternate, sustainable ways to contribute towards the conservation of the environment. Thus, the Indian knowledge system may continue to act as a tool for protecting the environment and in turn the human race, using green nanotechnology.

Received 24th January 2026
Accepted 12th May 2026

DOI: 10.1039/d6ra00662k

rsc.li/rsc-advances

1. Introduction

One of the major issues humanity faces today is environmental contamination driven by the uncontrolled exploitation of resources of toxic pollutants into the environment.[1] The textile sector primarily uses dyes, consuming over 80% of the total global dye production.[2] The untreated release of these colouring agents into environmental waters is ecologically harmful. Colour obstructs the dispersion of sunlight, inhibiting photosynthesis, and restricting the development of aquatic life.[2] Further, these dyes are highly poisonous, carcinogenic, non-biodegradable, and can also lead to numerous problems, including skin disorders and failure of the liver/kidneys.[2] Additionally, the usage of heavy metals in mining, electroplating, and other industries is also a cause of major environmental pollution. Heavy metal contamination is detrimental to both the environment and public health due to its long-term harmful effects. As a specific example, excessive lead (Pb) exposure can harm the kidneys, and affect reproductive and nervous systems. On the other hand, mercury (Hg) toxicity results in kidney and neural disorders.[3] Although iron is a required trace metal, its excessive levels can interfere with natural functioning and cause disorders such as hepatitis, arthritis, cancer, and heart failure.[4] Additionally, antibiotics are widely employed as medicine in both human beings and animals to treat inflammation caused by bacteria.[5] However, their excessive consumption and incorrect disposal can lead to the development of antibiotic resistance, digestive issues, and liver/kidney damage.[5] Furthermore, the use of various food colorants and additives is a growing concern in developing nations, harming the environment and public health.[6] Poor farmers have been reported to use malachite green (dye) to color vegetables, so that they appear fresh and green.[7] These dyes are hard to remove from vegetables, even after being washed, and may end up inside the body and eventually the food chain,

[a]*Department of Electronic Science, Bhaskaracharya College of Applied Sciences, University of Delhi, Delhi, India*

[b]*Department of Physics, Bhaskaracharya College of Applied Sciences, University of Delhi, Delhi, India*

[c]*Invited Researcher at Center for Research in Engineering and Applied Sciences (CIICAp-IICBA), Autonomous State University of Morelos (UAEM), Av. Univ. 1001, Col. Chamilpa, Cuernavaca, Morelos 62209, Mexico*

[d]*Center for Research in Engineering and Applied Sciences (CIICAp-IICBA), Autonomous State University of Morelos (UAEM), Av. Univ. 1001, Col. Chamilpa, Cuernavaca, Morelos 62209, Mexico. E-mail: vagarwal@uaem.mx*

[e]*Departamento de Fisico Matematica, UANL, Monterrey, Mexico*

leading to various diseases such as heart/respiratory failure, and even cancer. They may also damage the spleen, liver, and kidneys.

Various conventional techniques being employed for remediation of dyes from effluents involve adsorption, coagulation/precipitation, redox mechanisms, ion exchange, ultrafiltration (reverse osmosis), flocculation and biodegradation,[8] UV-light degradation, ozonation,[9] advanced oxidation,[10] electro/photochemical degradation[11] methods, high pressure liquid chromatography, surface-enhanced Raman spectroscopy (SERS),[12] enzyme-linked immunosorbent assay,[13,14] magnetic molecularly imprinted polymers.[1] Similarly, various analytical methods to identify heavy metals include X-ray fluorescence spectroscopy (XFS),[15] atomic emission spectroscopy (AES),[16] inductively coupled plasma-mass spectrometry (ICP-MS),[17] atomic absorption spectroscopy (AAS),[18] SERS and ion-selective electrodes.[19] However, these techniques suffer from many drawbacks including costly/complex instruments with tedious pre-/post-treatments requiring proficient operators and the creation of toxic by-products, *etc.* As a result, these procedures are sparingly used.

In contrast to the conventional techniques mentioned above, fluorescence (FL) sensors, utilizing nanomaterials, are presently being used because of their increased selectivity and sensitivity.[20,21] Although the primary focus has been on SnO_2, CdTe, and CdS-based semiconductor quantum dot fluorescent investigations, the incorporation of toxic heavy metals in these sensors lead to significant environmental and health risks.[4] Thus, designing metal-free, environmentally friendly sensors with high sensitivity is essential. In recent years, CDs have garnered substantial interest owing to their distinct characteristics, including facile surface functionalization, biocompatibility, and decreased toxic effects. They have been widely used for the detection of pollutants and other toxic chemicals due to their unique optical properties.[6] Furthermore, plant-based precursors are being investigated as an alternate carbon source for forming CDs, rather than chemical precursors,[22] due to their less toxicity, and being economically viable as well as environmentally sustainable.

2. Role of traditional Indian plants in environmental conservation

The ancient Indian knowledge system comprises of centuries old wisdom, which guides human beings to protect the

Fig. 1 Some typical traditional Indian plants utilized in the synthesis of CDs.

environment, generate awareness about their surroundings including plants, animals and water bodies. The foremost human community to protect the environment was the Vedic community, where humanity was aware of its surroundings.[23] In the Taittiriya Upanishad,[24] a set of guidelines are provided to maintain a clean environment. The significance of existence of each creature for the survival of all other creatures has been illustrated by the Iso-Upanishad.[25]

Trees secrete essential oils and secondary metabolites in defense, from its various parts such as leaf, bark, fruit, stem, flower, roots, or needles, which are natural bioactive compounds rich in steroids, flavonoids, polyphenols, tannins, xanthan, alkaloids, and terpenes, *etc.*[26–30] These compounds exhibit antioxidant, anti-inflammatory, antitussive, anti-diabetic, immunostimulant, antifertility, and anti-viral properties amongst others. Since ancient times, these bioactive compounds have been used in therapeutic applications[26,31] for treating numerous ailments such as diabetes, cancer, kidney and liver disorders, asthma, cardiovascular-related problems, fungal and bacterial diseases[32,33] and many more. The ancient Indian scientists documented a wide range of medications and treatments in Ayurveda and other ancient texts for maintaining good health and preventing diseases. Different plants are recognized on the basis of their characteristics and therapeutic advantages, which indicates our rich ancestral heritage and opulent knowledge of the plants' usage in daily life.

Recently, the usage of Indian traditional plants has increased for therapeutics, food, and craft purposes due to their nontoxicity and less side effects. For example, Bael plant, is included in the 'Climate Purifier' plant category, due to its behaviour of absorbing harmful gases from the atmosphere as well as sinking toxic chemical pollutants.[34] Mango, termed as the "National fruit of India" – is also known for its cardio protective, anticancer, anti-diabetic properties, *etc.*[33] Lotus is adopted as "National flower of India" used for ornamental, nutritional and medicinal properties.[35] Bamboo considered "Green Gold" is an inexpensive alternative to strong wood. It stores 1000 tonnes water, absorbs 12 tonnes of CO_2 gas, and releases 35% higher oxygen gas as compared to the deciduous forest trees.[36] Jackfruit is known as "giant nutrition fruit and a poor man's fruit"[37] whereas *Asparagus racemosus* (Shatavari) is taken as 'adaptogens' for supporting the body to handle different types of stresses.[27] The United Nations have declared *Azadirachta indica*, (neem) as "Tree of the 21st century" due to its versatile usage as a traditional Indian medicine for various diseases.[30] Furthermore, these historic pieces of knowledge have inspired innovative research and improvements in health care and our surroundings. Fig. 1 shows some of the traditional Indian plants that have been used in the synthesis of CDs.

3. Synthesis and characterization of CDs using plant-based biomass

The fabrication of carbon dots from natural precursors represents a novel and eco-friendly approach in the diverse field of nanotechnology, employing accessible and environmentally sustainable materials, including vegetables, fruits and extracts from different parts of plants. Natural precursors provide a substantial carbon source and possess intrinsic biological compatibility, making them suitable for the synthesis of CDs with a reduced environmental impact.

The synthesis of carbon dots (Fig. 2) predominantly employs a bottom-up approach, where the green precursors are carbonized either through hydro/solvo-thermal[38,39] techniques or methods assisted by microwaves[40] or ultrasonics. Hydrothermal/solvothermal synthesis involves the application of elevated temperatures and pressures to organic precursors in an aqueous/solvent solution, yielding CDs characterized by well-defined sizes and surface functionalization.[39] Similar to this, microwave-assisted synthesis produces CDs quickly and effectively by irradiation with microwaves which escalates the carbonization process. Microwave synthesis is primarily attractive due to its capacity for rapid, energy-efficient heating, which results in reduced response times and enhanced control over morphology of particles.[41] This synthesis procedure employs sources of carbon (glucose, citric acid,[42] or other organic materials), forming their solution, and then subjecting microwave irradiation. Rapid dielectric heating results because of interaction of the microwaves with the polar molecules. This process ensures satisfactory product quality with little agglomeration by promoting homogeneous nucleation and development of CDs in addition to speeding up chemical processes. Apart from the concentration of the green precursor, the main variables that control the synthesis process are the duration and power of irradiation. The ease of application and scalability of microwave-assisted synthesis make it a noteworthy approach.

The use of ultrasonic waves represents an innovative method in nanotechnology, utilizing the distinctive advantages of ultrasound-assisted technique. Using high-frequency sound waves, the ultrasonic approach for CD synthesis creates vapor filled voids/bubbles in water/solvent containing green precursors. The collapse of these bubbles helps in creating high pressure & temperature locally, which promotes the formation of nanosized carbon particles from the fragmentation of carbon. This procedure offers advantages such as simplicity, cost-effectiveness, environmental sustainability, facilitating scalability, and high efficiency for producing CDs with adjustable characteristics.[43,44] Several important parameters, including temperature, sonication power, and sonication time, can be optimized to greatly increase the yield of CDs produced using ultrasonic waves. On the other hand, in conventional pyrolysis, carbon source materials are thermally broken down to create CDs using temperatures, usually between 300 and 1000 °C, in an oxygen-free atmosphere.[45] In this process, organic molecules experience carbonization and cracking, leading to the formation of carbon core and some functional groups on the surface (depending on the temperature). Fig. 2 depicts various synthesis methods of CDs using natural biomass and their main applications (colorimetric/optical sensing/photocatalytic degradation/electrochemical sensing *etc.*).

Fig. 3 shows the main characterization techniques used for the analysis of carbon dots (CDs), which enable the correlation of their physicochemical properties with their performance in

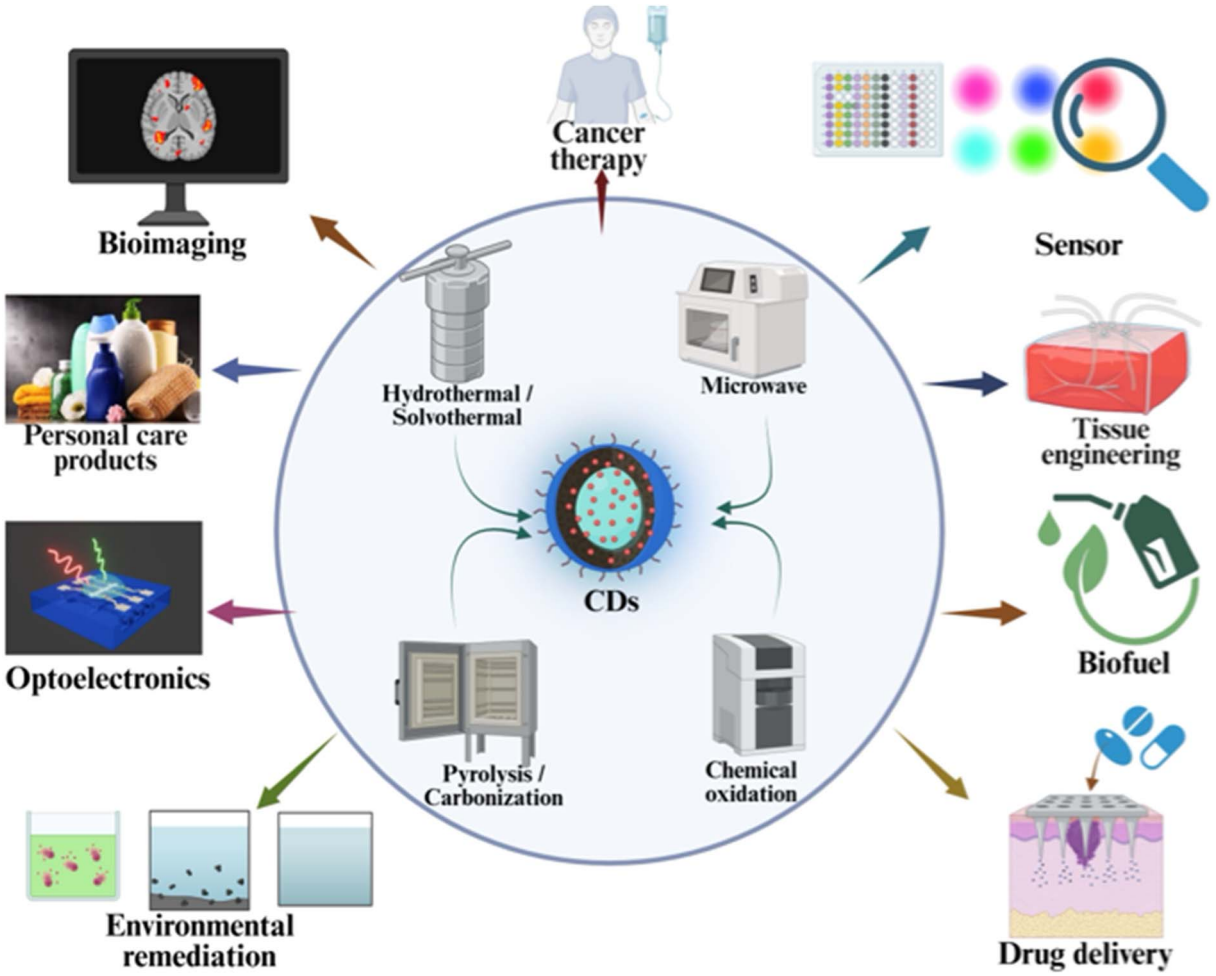

Fig. 2 Some main green synthesis techniques (inner circle) and applications of CDs synthesized using natural precursors.

various applications. Morphological and structural characteristics are generally evaluated by high-resolution scanning (HRSEM)/transmission electron microscopy (HRTEM). These techniques are used for finding the particle size, shape, and the degree of aggregation of CDs, with high resolution. In particular, TEM is widely used to observe the internal structure and possible crystalline domains, as well as to estimate the average size at the nanometric scale. On the other hand, SEM provides complementary information on surface morphology and the distribution of nanoparticles in different matrices.[46–48] Additionally, Atomic Force Microscopy (AFM) enables the analysis of surface features and the measurement of the height of CDs, which is especially useful for confirming their quasi-spherical nature and their vertical dimension, providing three-dimensional information at the nanometric scale.[49]

The crystalline structure and degree of ordering of CDs are studied using X-ray diffraction (XRD), a technique that allows the identification of graphitic or amorphous structures, as well as the estimation of parameters such as interplanar spacing.[46,48] Furthermore, the chemical composition and the nature of functional groups on the surface are determined by infrared spectroscopy[3] (FTIR) and X-ray photoelectron spectroscopy (XPS). FTIR enables the identification of characteristic vibrational modes associated with specific bonds/groups such as O–H, C=O, C=S, C–O, –NH_2, –COOH, evidencing the presence of oxygen and heteroatoms that influence the solubility and reactivity of CDs. Complementarily, XPS provides detailed elemental composition and the presence of oxidation states of the atoms, allowing for a more detailed analysis of surface chemistry and doping mechanisms.[46,50]

The optical characteristics of CDs are analyzed using UV-Vis and photoluminescence (PL) spectroscopy, which are fundamental techniques for understanding their light absorption and emission mechanisms. UV-Vis spectroscopy allows the identification of characteristic electronic transitions, such as π–π^* and n–π^* transitions, associated with conjugated structures and surface functional groups.[3,46,48,50] Meanwhile, PL provides information on electron recombination processes and emissive centers, being particularly relevant for evaluating phenomena such as excitation wavelength-dependent emission, quantum yield, and the influence of surface defects.[50,51] Likewise, zeta potential is used to evaluate the colloidal stability and surface charge of CDs in dispersion. This parameter is crucial for understanding electrostatic interactions between particles, as

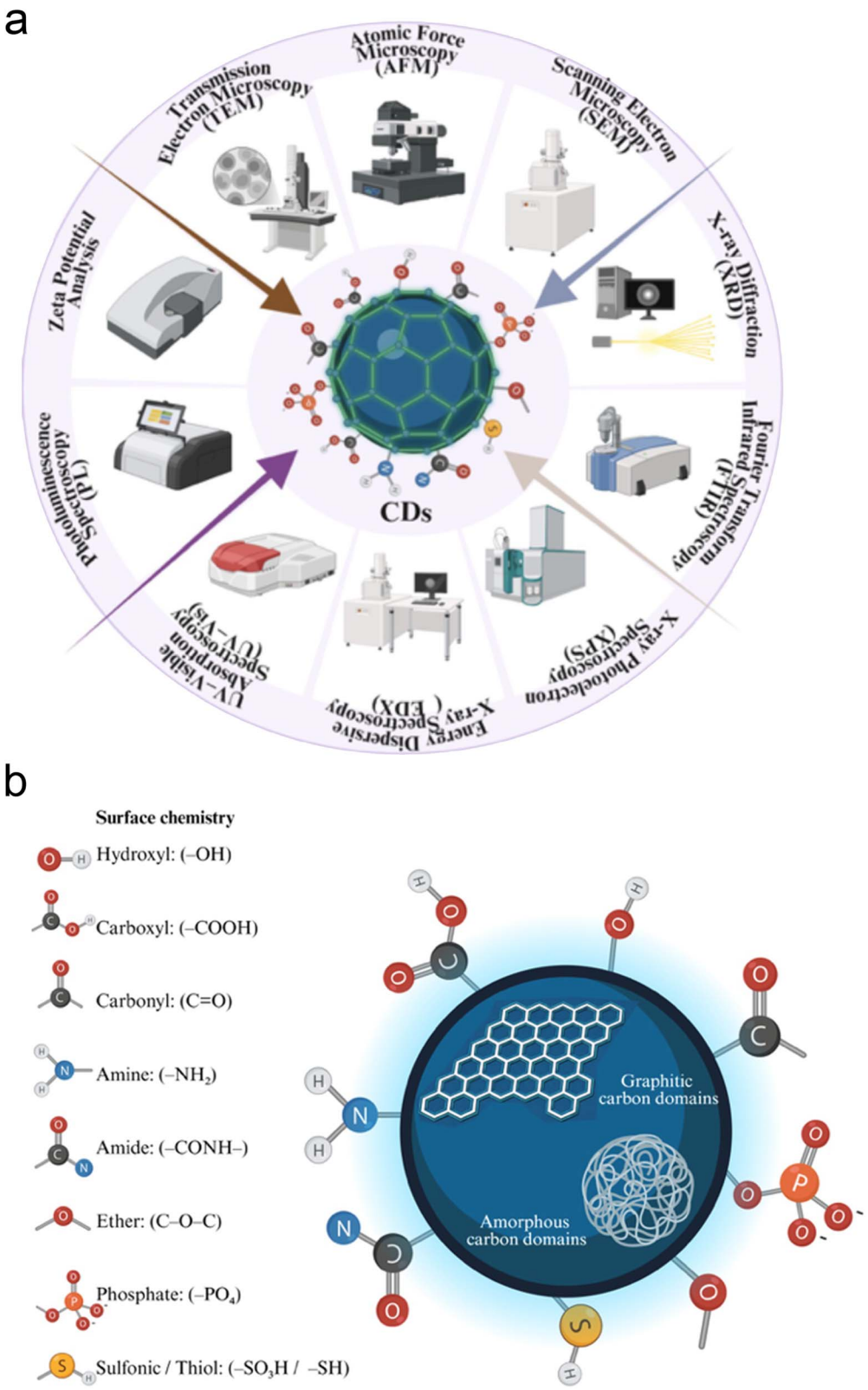

Fig. 3 (a) Schematic representation of some common characterisation techniques employed for CDs. (b) Typical functional groups associated with doped and undoped CDs.

well as their behavior in aqueous media and biological systems, directly influencing their aggregation, dispersibility, and applications in sensing or bioimaging.[46,48,50]

Overall, the integration of these characterization techniques enables the establishment of a comprehensive correlation between the structure, surface chemistry, and optical properties of CDs.

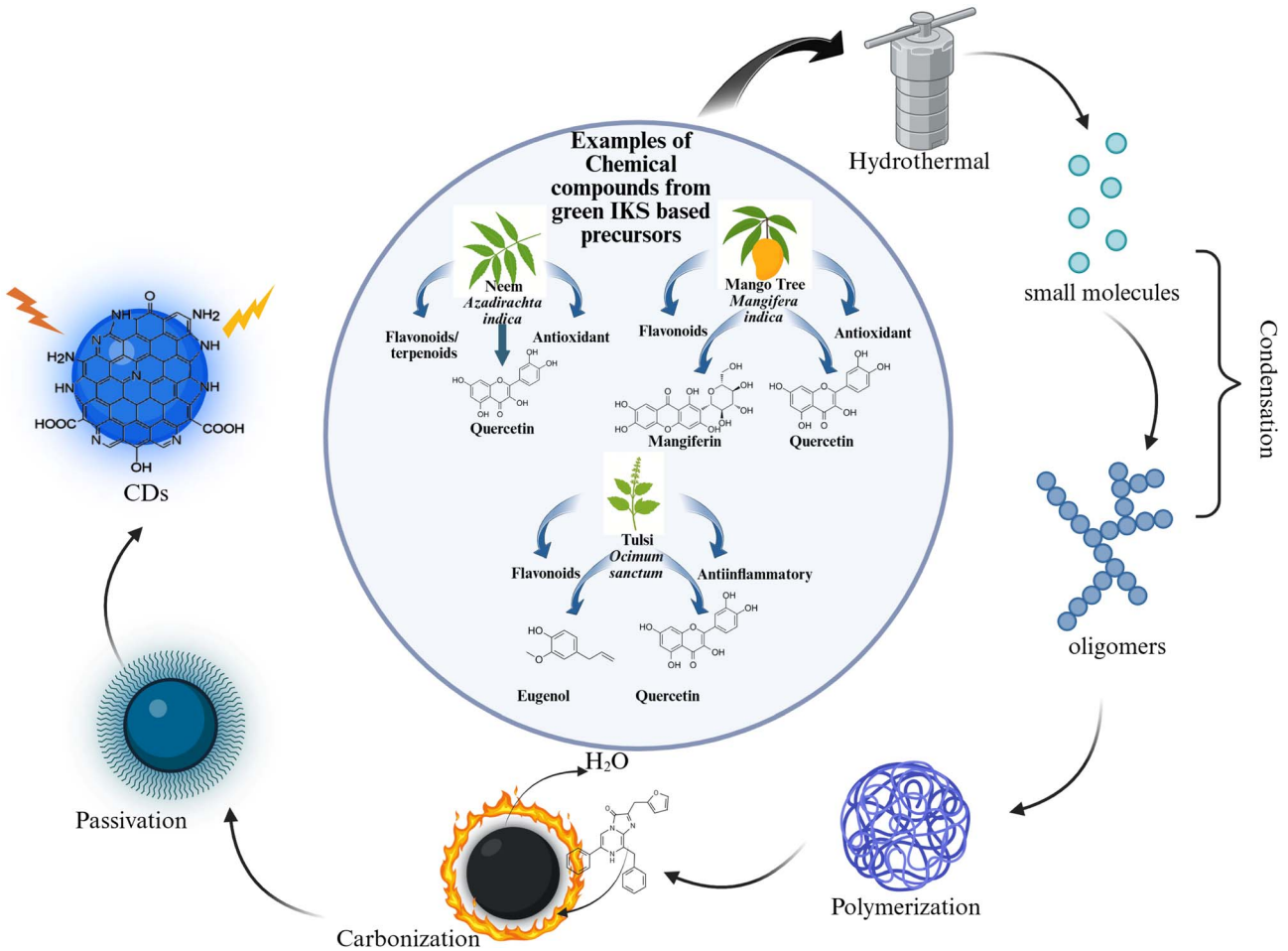

Fig. 4 Schematic representation of the possible formation mechanism of CDs showing different stages.

4. Formation mechanism of CDs

The design of novel carbon dots with the required properties demands a deep understanding of their formation mechanism. Due to the simultaneous involvement of several variables, including reaction time, temperature, and precursor structure, it is an intricate task that requires systematic studies. In the detailed work from Rigodanza *et al.*,[52] it has been shown that the formation of carbon dots consists of four different stages, involving aggregation, shell formation, collapse, and aromatization.

Similarly, the formation mechanism of CDs *via* the bottom-up technique has been shown to involve the carbonisation of small organic matter. This is achieved through a number of steps, including condensation, polymerisation, carbonisation followed by surface passivation.[53] The tiny molecules go through the condensation processes like aldol condensation,[54] Schiff base condensation,[55] amidation[56] and radical reaction,[57] leading to the formation of chain-like intermediaries, which further lead to the creation of polymer like CDs.[58] The polymers subsequently get carbonised, generating the carbon core, particularly at high temperatures.[59,60] Furthermore, the remaining precursors, serving as surface passivating agents, can be altered on their surface to increase the luminescence of CDs. Research on doped and hybrid CDs, such as N, S-co-doped CQDs and Gd-doped CQDs, demonstrates that nuclei formation, growth, and carbonisation are significantly influenced by temperature and time[61,62]

Sustained microwave irradiation encourages intramolecular dehydration and C–C bond creation in palm kernel shell-derived CDS, generating aromatic functional groups and facilitating CD nucleation. The most acceptable formation mechanism is depicted in Fig. 4. Some specific examples of the precursors from IKS, along with their corresponding medicinal value as per the ancient texts and bioactive compunds are given in Table 1. The synthesis parameters and some resulting characteristics are also listed.

5. Origin of photoluminescence

Although origin of the photoluminescence (PL) mechanism has been vividly explored, it is still not entirely understood owing to the wide variety of precursors and techniques being adopted during the synthesis, exhibiting the formation of a complex

Table 1 Optimized synthesis conditions and results obtained from various characterisation studies in plant (from IKS)-based biomass. The functional groups and chemicals present have been specifically highlighted

S. no.	Precursor/plant family	Medicinal/general usage	Bioactive compounds present	Synthesis method/ optimised synthesis conditions (temperature/ duration/pH)	Dopant used	Characterisation techniques	Size (nm)/zeta potential	Functional groups reported
01	Curry leaves extract[3,26](*Murraya koenigii*)/Rutaceae	Anti-bacterial, anti-inflammatory, anti-dysenteric, anti-diabetic, carminative and digestive properties	Vitamin C & A, essential oils α-terpinene sabinene, α-pinene, β-pinene, iron, phosphorus, magnesium oxalates, terpenoids, alkaloids, fiber	Microwave/800 W for 8 min	—	UV-Vis spectroscopy, FTIR	—	–OH, C=C, C=O, C–O, C–H, COOH
02	Giloy stem[28,46] (*Tinospora cordifolia*)/ Menispermaceae	Chronic fever, dengue fever (increases platelet count), virus infection, hay fever, improve digestion, boost immunity, reduces stress and anxiety, treats arthritis/gout, leprosy, anorexia, jaundice, diuretic, astringent, itching, bleeding piles, erysipelas, memory booster	Steroids, alkaloids, polysaccharides, glycosides, terpenoids, and lignans	Hydrothermal/160 ° C for 5 h, pH = 5.6	Alkaloids (N source), terpenoids (C source), steroids (S source)	TEM, DLS, XRD, XPS, FTIR, zeta potential, UV-Vis & fluorescence spectroscopy, time-resolved fluorescence (lifetime)	3–7/−10.7 mV	C=C, C–H, C–C, C–N–C, C–O–C, C=O, N–C_3, N–H, –NH_2, C–S, S=O, C=S, –OH, COOH, COSH
03	“Shatavari” *Asparagus racemosus* root[27,48] (Asparagaceae)/ (Liliaceae)	Described as ‘rasayana herb’; anti-lung cancer activity, phytoestrogenic, anti-bacterial, cardio protective, anti-dyspepsia, anti-diarrhoeal, adaptogenic, antiaging, promoting intellect, physical strength, immunoadjuvant, used for neurodegenerative disorders	Steroidal saponins (shatavarin I–IV), quercetin, rutin, hyperoside, diosgenin, quercetin-3, glucuronide	Microwave/900 watts at 10 min	—	TEM, XRD, UV-Vis & fluorescence spectroscopy, FTIR, zeta potential	8/−48.4 mV	–OH, –COOH, C=O, C–H, N–H

Table 1 (*Contd.*)

S. no.	Precursor/plant family	Medicinal/general usage	Bioactive compounds present	Synthesis method/ optimised synthesis conditions (temperature/ duration/pH)	Dopant used	Characterisation techniques	Size (nm)/zeta potential	Functional groups reported
04	Neem seeds (*Azadirachta indica*[50,63])/ Meliaceae	Biopesticides insecticidal, fumigant, manure, urea coating agent, soil conditioner, anti-viral, anti-fungal, anti-bacterial	Limonoids group (triterpenoids) including nimbin, azadirachtin, nimbidin, salannol, salanin, gedunin, quercetin	Hydrothermal carbonization/180 °C for about 12 h	Aqueous NH_3 (as N source)	HR-TEM, SAED, XRD, XPS, FTIR, EDS, Raman spectroscopy, UV-Vis spectroscopy, fluorescence spectroscopy, zeta potential, TGA	2.5/−20.4 mV	–OH, –NH_2, –C=C, C–N, NH, –COOH, C=O, C–O–C
05	Neem leaves[30,64] (*Azadirachta indica*)/ Meliaceae	Biopesticides, insecticidal, fumigant, manure, urea coating agent, soil, conditioner, anti-viral, anti-fungal, anti-bacterial	Limonoids group (triterpenoids) including Nimbin, Azadirachtin, Nimbidin, salannol, salanin, gedunin, quercetin	Pyrolysis and hydrothermal/ hydrothermal (i) 180 °C for 2 h/pH = 7.4 200 °C for 12 h	—	HRTEM, AFM, XRD, XPS, FTIR, SAED, EDX, UV-visible spectroscopy, photoluminescence (PL) spectroscopy	2.5/−20.4 mV	–OH, –NH/NH_2, –COOH, C=O, –$CONH_2$, –C–NH_2
06	Black plum leaves[4,65] (*Syzygium cumini*)/Myrtaceae	Cancer, diabetes, diarrhea, leucorrhea, stomach pains, increased hemoglobin, skin health improvement	Glycosides, myricetin, ellagic acid, flavonol, caffeic acid beta-sitosterol, alkaloids, flavonoids, steroids, phenols, and tannins	Hydrothermal/180 °C for 2 h/pH = 7.4	O & N groups derived from phytochemicals	HRTEM, FTIR, XPS, UV-Vis spectroscopy, fluorescence lifetime spectroscopy (FLS), zeta potential	3.4/−14.3 mV	–OH, –COOH, C=O, C–O, –NH2, –N–H
07	Jamun fruit[66] (*Syzygium cumini*)/ Myrtaceae	Cough, diabetes, inflammation dysentery, gastrointestinal complaints, ringworm	Quercetin, rutin, ferulic	Hydrothermal/180 °C for 6 h/pH = 5.0	—	HRTEM, DLS, UV-Vis spectroscopy, fluorescence spectroscopy, FTIR, confocal laser microscopy	2.1 ± 0.5/—	–OH, C=O, –COOH, –NH_2, –CO, C–N, –CHO
08	Pinewood (*Pinus*)[32,67]/ Pinaceae/O & N groups derived from phytochemicals	Kidney/liver disorders, cancer, asthma, diabetes, cardiovascular problems, antihypertensive, fungal/bacterial diseases	Alkaloid, tannins, flavonoids, alkaloids, terpenoids cellulose, hemicellulose and lignin	Hydrothermal carbonisation/180 °C for 3 h	O & N groups derived from phytochemicals	HRTEM, AFM, UV-Vis & PL spectroscopy, XPS, FTIR	3.56/—	–OH, –COOH, C=O, C–O–C, –NH
09	Pine needles[47]/ Pinaceae	Kidney/liver disorders, cancer, asthma, diabetes, cardiovascular problems, antihypertensive, fungal/bacterial diseases	Alkaloid, tannins, flavonoids, alkaloids, terpenoids cellulose, hemicellulose and lignin	Hydrothermal/200 °C at 6 h/pH = 7.0	Natural C & N source	HRTEM, SEM, DLS, XRD, FTIR, Raman spectroscopy, TGA, UV-Vis spectroscopy	3.56 ± 0.85/—	–OH, C=O, –NH, –COOH, C–O, C–C, C–N, C=C

Table 1 (*Contd.*)

S. no.	Precursor/plant family	Medicinal/general usage	Bioactive compounds present	Synthesis method/ optimised synthesis conditions (temperature/ duration/pH)	Dopant used	Characterisation techniques	Size (nm)/zeta potential	Functional groups reported
10	Pinecones and pine bark[5]/Pinaceae	Kidney/liver disorders, cancer, asthma, diabetes, cardiovascular problems, antihypertensive, fungal/bacterial diseases	Alkaloid, tannins, flavonoids, alkaloids, terpenoids, cellulose, hemicellulose and lignin	Microwave pyrolysis at 1000 W for 1 h/pH = 4	—	TEM, HRTEM, SEM, DLS, XRD, FTIR, Raman spectroscopy, TGA, UV-Vis spectroscopy	19.2 (PCCD) 18.39 (PBCD)/—	–OH, –COOH, C=O, C–O–C–CH_2, –OCH_3, H–N
11	Tamarind leaves[33,51] (*Tamarindus indica)* (blue light emitting CDs, b-CQD) & mango leaves (*Mangifera indica*) (green light emitting CQDs; g-CQDs)	Anti-asthmatic, antidiabetic, deep wounds, high fever, malaria, blood related diseases, digestive issues, cardiovascular disorders, anti-venomous, hepato-protective, analgesic, anti-inflammatory and parasitic potentials	Xylose, pectin, glucose, galactose and uronic acid, tartaric acid, tannin, sugars, fiber, protein, carbohydrates Ca, K, Zn, Fe, Na	Microwave: h-CQDS blue-emitting CQDs (b-CQDs) 210 °C for 5 h green-emitting CQDs (g-CQDs) 180 °C for 4 h	—	UV-Vis spectrophotometry, PL spectroscopy, smartphone-based fluorometry, statistical and empirical modeling	—	For g-CQDs: C=C, C=O, C–O–C, R-COOH, $RCONH_2$ RCOOR and for b-CQDs: C=C, R-COOH, $RCONH_2$, RCOOR
12	Tamarind shell waste[68] (*Tamarindus indica*)/ Leguminoaes	Anti-asthmatic, antidiabetic, deep wounds, high fever, malaria, blood related diseases, digestive issues, cardiovascular disorders, anti-venomous, hepato-protective, analgesic, anti-inflammatory and parasitic potentials	Xylose, pectin, glucose, galactose and uronic acid, tartaric acid, tannin, sugars, fiber, protein, carbohydrates Ca, K, Zn, Fe, Na	Carbonization at 400 °C followed by microwave irradiation for 30 min/pH = 7.0 (CQDs) pH = 12.0 (ZnO)	Nanocomposite CQDs/ZnO	XRD, TEM, HRTEM, FE-SEM, EDX, FTIR, Raman spectroscopy, UV-visible spectroscopy, XPS	40–55 (Photocatalyst)/—	–OH, C–O–C, C–O, C=O
13	Lotus root[35,69] (*Nelumbo nucifera*)/ Nelumbonaceae	Ornamental value; antimicrobial, antibacterial, antifungal, anti-plasmodial, antioxidant, skin infections, reproductive and respiratory diseases	Alkaloids, glutathione, mucilaginous juice, iso-quercetin, amino acids, glucoprotein, polysaccharides, glucoluteolin, starch, asparagines, methanolic extract	Microwave/pH 7.0	N groups derived from phytochemicals	TEM, FTIR, XPS, UV-Vis absorption & fluorescence spectroscopy, fluorescence lifetime measurement	9.41/—	–OH, NH_2, –C–N, –COOH, C=O, C–H

Table 1 (*Contd.*)

S. no.	Precursor/plant family	Medicinal/general usage	Bioactive compounds present	Synthesis method/ optimised synthesis conditions (temperature/ duration/pH)	Dopant used	Characterisation techniques	Size (nm)/zeta potential	Functional groups reported
14	Teak leaves[70,71] (*T. grandis* Linn.)/ Verbenaceae	Bronchitis, hyperacidity, biliousness, leprosy, diabetes, helminthiasis, swellings, astringent paste for wounds	Phenols and phenolic acid, norlignans, flavonoids, anthraquinones, glycosides, alkaloids, terpenoids, apocarotenoids, steroids, lignans	Ultrasonication (at 40 kHz)	—	UV-Vis absorption, FTIR, Raman spectroscopy, XRD, HRTEM, FESEM, EDAX, zeta potential analysis	5/−51.0 mV	–OH, –CH, =C–H, C–O–C, C=O, COO–
15	Tulsi leaves[72,73] (*Ocimum sanctum*)/ Lamiaceae	Common cold/cough/ flu (influenza), headache, earache,	Eugenol, flavonoids, phenolics, gallic acid, vallinin, terpenoids,	Hydrothermal, 180 °C for 4 h/pH 7.0	—	FTIR, XRD, TEM, FESEM, UV-Vis absorption, PL spectroscopy, EDAX	3/—	–OH, C=C, C–H, –NH, C–N, –COOH, C=O
16	Tulsi leaves *Ocimum tenuiflorum*[6]	colic pain, asthma, hepatic diseases, insomnia, malaria fever, ulcer, arthritis, night blindness,	oleic acid, palmitic acid, linoleic acid	Hydrothermal 200 °C for 12 h	—	DLS, TEM, Raman spectroscopy, FTIR, XPS, SAED, zeta potential, UV-Vis and fluorescence spectroscopy	1–3/−18 mV	–OH, N–H, C=O, COO–, C=C, C–N, C–H, C–O–C
17	Tulsi leaves[74]	digestive disorder, memory enhancer		Hydrothermal 200 °C for 4 h	—	TEM, EDX, XRD, FE-SEM, TGA, FTIR, zeta potential, UV-Vis spectroscopy, time resolved fluorescence decay	5/−25.7 mV	C=O, C=C, –OH, =N–H, C–H
18	Lily jasmine[75,76] or motia leaves (*Jasminum sambac*)/ Oleaceae (i) (CDs-MnO_2) (ii) (NCDs-MnO_2)	Antiulcer, antioxidant activities, breast cancer, dermatitis, diarrhea, conjunctivitis, fever, asthma, abdominal pain, toothache abscess, uterine bleeding	Flavonoids, alkaloids, phenols, terpenoids, carbohydrates, tannins, proteins, phytosterols, saponins, resin, steroids, salicylic acid	Ultrasonic radiation assisted synthesis	Aq. NH_3 as N dopant	UV-visible spectrophotometry, FTIR, XRD, EDX, SEM	(i) 22.04/—	–OH, C≡C, C–O, Mn–O
							(ii) Amorphous	–CH, C=C
19	Indian jujube fruit (*Ziziphus mauritiana*)[77,78]/ Rhamnaceae	Sedative, hepatoprotective, antimicrobial, hypoglycemic, anti-plasmodial, antidiabetic, anti infectious, analgesic, diuretic, anti-inflammatory and anticonvulsant, useful in old wounds, ulcers diarrhea, antipyretic, anti-obesity, blood purifier, digestion, respiratory disorders	Phenolic compounds flavonoids, alkaloids, terpenoids, lipids, triterpenoic acids, saponin, pectin	Hydrothermal 200 °C for 8 h/pH = 12	Aq. NH_3 as N dopant	UV-Vis, FTIR, Raman, XRD, XPS, HR-TEM	7.4 ± 1.6/—	–NH, –OH, –C=C, –C–O–C

Table 1 (*Contd.*)

S. no.	Precursor/plant family	Medicinal/general usage	Bioactive compounds present	Synthesis method/ optimised synthesis conditions (temperature/ duration/pH)	Dopant used	Characterisation techniques	Size (nm)/zeta potential	Functional groups reported
20	Indian jujube fruit[79] (*Ziziphus mauritiana* pulp extract)/ Rhamnaceae	Sedative, hepatoprotective, antimicrobial, hypoglycemic, anti-plasmodial, antidiabetic, anti infectious, analgesic, diuretic, anti-inflammatory and anticonvulsant, useful in old wounds, ulcers diarrhea, antipyretic, anti-obesity, blood purifier, digestion, respiratory disorders respiratory disorders	Phenolic compounds flavonoids, alkaloids, terpenoids, lipids, triterpenoic acids, saponin, pectin	Hydrothermal 190 °C for 5 h/pH = 7.0	N groups derived from phytochemicals	XRD, UV-visible spectroscopies, SEM, EDX, PL, TEM, FTIR	2.54/−18.7 mV	C–O, C–N, –OH, C–H, N–H, C=C, C=O
21	Mango peels (*Mangifera indica*)[80,81]/ Anacardiaceae	Anti-asthmatic, anti-diabetic, deep wounds, malaria, blood-related diseases, digestive issues, cardiovascular disorders, anti-venomous, hepato-protective, analgesic, anti-inflammatory, anti-oxidant, anticancer, anti-microbial	Carotenoids polyphenols, omega-3 and -6 polyunsaturated fatty acids, phytochemicals, micronutrients, fibre vitamins, carbohydrates, proteins, phenolic compound	Hydrothermal, 200 °C for 4 h/pH = 8	Composite of CDs with molecularly imprinted polymers; CQDs@MIPs	FL spectroscopy, FTIR, UV-Vis, TEM, SEM, AFM, XPS, XRD, FL life time	3–5 nm/—	C–H, –OH, =C–O, –COOH, –OH, $–NH_2$, C=O
22	Bael patra fruit[82,83] (*Aegle Marmelos*)/ Rutaceae (i) C-CDs (peel-hard shell) (ii) P-CDs (edible pulp) (iii) M-CDs/(mixture of pulp and gum)	Antioxidant, anticancer, anti-plasmodial, antimicrobial, hepatoprotective activities	Marmelosin, coumarins, marmenol, imperatorin, xanthotoxin, methyl ether, scoparone, umbelliferone, scopoletin, psoralen marmeline	Hydrothermal 180 ° C for 12 h/pH = 7.0	Aq. NH_3	HRTEM, BET, FESEM, FTIR, XPS, UV-Vis spectrophotometry, zeta potential	(i) 3 nm/+0.23 mV (ii) 6 nm/+ 0.11 mV (iii) 8 nm/+0.07 mV	C–N, C=O, =N–H, –OH, –COOH, C–H, C–O

Table 1 (*Contd.*)

S. no.	Precursor/plant family	Medicinal/general usage	Bioactive compounds present	Synthesis method/ optimised synthesis conditions (temperature/ duration/pH)	Dopant used	Characterisation techniques	Size (nm)/zeta potential	Functional groups reported
23	Dwarf banana peel[84,85] (*Musa acuminata*)/ Musaceae	Antioxidant, anti-diabetic, immunomodulatory, hypolipidemic, anticancer, anti-microbial properties anti-hypertensive, anthelmintic, tuberculosis, respiratory diseases	Terpenoids, saponins, steroids, alkaloids, anthocyanins, tannins, fatty acids, phenols, steryl esters, sterols, polyphenols, fiber, flavonoids, lignin, lipids, hemicellulose, minerals proteins, cellulose	Hydrothermal/200 °C for 24 h	Aq. NH_3	XRD, Raman spectroscopy, HRTEM, XPS, ATR-FTIR, PL spectroscopy	4/—	–COO, –OH, C–OH, –COOH C–O–C, $–NH_2$, –C–NH
24	Pseudostem of banana[86] (*Musa acuminata*)/ Musaceae	Antioxidant, anti-diabetic, immunomodulatory, hypolipidemic, anticancer, anti-microbial properties anti-hypertensive, anthelmintic, tuberculosis, respiratory diseases	Terpenoids, saponins, steroids, alkaloids, anthocyanins, tannins, fatty acids, phenols, steryl esters, sterols, polyphenols, fiber, flavonoids, lignin, lipids, hemicellulose, minerals proteins, cellulose	Hydrothermal/180 °C for 2 h/pH = 7.4	—	UV-Vis, fluorescence, DLS, FT-IR, Raman, XPS, HRTEM	2.51/—	–OH, C=C, C=O, C–O–C
25	(i) Ripe banana peels[87] (BCD_{BP}) (ii) Dried rose petals (BCD_{RP}) (iii) Biochar	Antioxidant, anti-diabetic, immunomodulatory, hypolipidemic, anticancer, and antimicrobial properties, anti-hypertensive, anthelmintic, tuberculosis, respiratory diseases	Terpenoids, saponins, steroids, alkaloids, anthocyanins, tannins, fatty acids, phenols, steryl esters, sterols, polyphenols, fiber, flavonoids, lignin, lipids, hemicellulose, minerals proteins, cellulose	Hydrothermal/180 °C for 6 h	(i) Ethylenediamine + L-cysteine (ii) Ethylene diamine + L-cysteine	XRD, Raman spectroscopy, HRTEM, XPS, ATR-FTIR, PL spectroscopy	(i) 9.5/— (ii) 7.2/—	$O–CH_3$, –C–O, OCH_2, –OH, –C=O, C=C, COOH, C–H, –SH, =NH
26	Betel leaves[49,88] (*Piper betle*)/ Piperaceae	Antimicrobial, antioxidants, antifungal, anticancer, anti-inflammatory, anti-diabetic and digestive and gastroprotective characteristics	Calcium, minerals, vitamin C, niacin, carotene, thiamine and riboflavin	Hydrothermal 200 °C for 12 h	N groups derived from phytochemicals	XRD, Raman spectroscopy, TGA, DTA, XPS, TEM, HRTEM, FTIR, UV-Vis and fluorescence spectroscopy	~4/—	–OH, =NH, C–H, C=O, C=C, C–N, C–OH, C–O–C, $–CH_2$, –COOH, C=N, $–NH_2$, C–C, C–N–C, –CONH –OH,
27	Betel leaves[88] (*Piper betle*)/Piperaceae		Alkaloids, flavonoids, tannins, saponins, chavicol, diastase, essential oil	Hydrothermal 180 °C for 12 h/pH = 7	+Ammonia solution (N-dopant)	AFM, HR-TEM, PSA, XPS XRD, FTIR, UV-Vis spectroscopy, fluorescence spectroscopy with lifetime analysis	3.7/—	–NH, –CONH, $N–C_3$, C=O, C=N, C–O, C–N, C–N–C

Table 1 (*Contd.*)

S. no.	Precursor/plant family	Medicinal/general usage	Bioactive compounds present	Synthesis method/ optimised synthesis conditions (temperature/ duration/pH)	Dopant used	Characterisation techniques	Size (nm)/zeta potential	Functional groups reported
28	Bamboo leaves[89,90] (*Bambusa vulgaris*)/ Poaceae	Paper making, construction (bamboo bridges/railings, living hedges, household items/furniture, tiles *etc.*), medicinal virtues, religious purposes, educational purposes, ornamental purposes and landscape gardening, containers, seed drills	Proteins, amino acids, carbohydrates, minerals, vitamins, phytosterols, fibre, phenols, glycosides	Solvo-thermal 180 °C for 5 h	—	TEM, FTIR, XPS, UV-Vis and fluorescence spectroscopy	3–7/—	C–O, C–N, –OH, C–C, C–H, N–H, C=O
29	Bamboo leaves[91] branched polyethylenimine (BPEI)-capped CQDs (BPEI-CQDs)	Paper making, construction (bamboo bridges/railings, living hedges, household items/furniture, tiles *etc.*), medicinal virtues, religious purposes, educational purposes, ornamental purposes and landscape gardening, containers, seed drills	Proteins, amino acids, carbohydrates, minerals, vitamins, phytosterols, fibre, phenols, glycosides	Hydrothermal/200 °C for 6 h	—	FTIR, UV-Vis and FL spectroscopy, TEM, zeta potential	3.6/+13.8 mV	COOH, –OH, C=O
30	Pomegranate juice[92,93] (*Punica granatum* L.)/ Lythraceae	Anticancer, stomach disorder, diarrhea, cardiovascular problems, osteoarthritis, diabetes, dental care, anemia	Vitamins (C, K and folate), seed oil, antioxides, polyphenols, ellagitannins, anthocyanins, delphinidin, cyanidin, and pelargonidin glycosides, flavonoids	Hydrothermal 120 °C for 5 h/pH = 5–9	Ammonium hydroxide	UV-Vis absorption, FTIR, HRTEM, XPS	2–5/+ 20.97 mV	=NH, C–H, –OH, COO–, C–OH, C–O–C, C–N

Table 1 (*Contd.*)

S. no.	Precursor/plant family	Medicinal/general usage	Bioactive compounds present	Synthesis method/ optimised synthesis conditions (temperature/ duration/pH)	Dopant used	Characterisation techniques	Size (nm)/zeta potential	Functional groups reported
31	Jackfruit seeds[94,95] (*Artocarpus heterophyllus*)/ Moraceae	Antioxidant, anti-inflammatory, antihypertensive, antibacterial, antifungal, anticarcinogenic, antineoplastic; also used in preparation of bakery items breakfast cereals, and infant food	Fibre, proteins, carbohydrates, vitamins, minerals (Mg, K, P, Ca, Na, Fe, C, Zn, Mn) phenolics, flavonoids, terpenoids, steroids, glycosides, saponins, carotenoids, sterol, alkaloids, tannin	Microwave-assisted; 600 W for 1 m & 30 s	—	XRD, TEM, SAED, zeta potential, HRTEM, FTIR, XPS, Raman spectroscopy, UV-vis absorption, PL spectroscopy	5/−43.2 mV	–OH, N–H, C=O, COO–, C=C, C–O
32	Gum Ghatti[96,97] (a natural exudate from *Anogeissus Latifolia* tree/ Combretaceae	Emulsions, suspensions, sizing agent in the paper industry, house construction, treatment of piles, diarrhea, respiratory diseases, liver issues	Tannin, sugars, its nature as a calcium–magnesium salt	Microwave pyrolysis (20 minutes)	—	XRD, XPS, TEM, FESEM, FTIR, UV-Vis spectroscopy, PL spectroscopy	2.6/—	–OH, –CH, C–O, C=C, C=O, C–O–C, C–N
33	Turmeric powder[98,99] Zingiberaceae	Anti-inflammatory, antiseptic, disinfectant, analgesic, aiding digestion, skin treatment	Alkaloid, curcuminoi-dflavonoids, amino acids, phenolics, protein	Hydrothermal 200 ° C for 24 h	—	XRD, SEM, TEM, FTIR, vibrating sample magnetometer (VSM), UV-Vis absorption, PL spectroscopy	20–100/—	C=O, –OH, C–O, C–H, –COOH
34	(i) Azadirachta indica (NNP)[100]	(i) Therapeutic and biological properties, antioxidant properties	(i) NNP-nimbolide, azadirachtin, ascorbate	Microwave 800 W for 3 min/80 °C for 12 h		XRD, FESEM, EDX, FTIR, UV-Vis spectrophotometry	(i)33/—	(i) C=N, –OH, C–H, C≡N, C–O, C–N
	(ii) Psidium guajava (GuNP)	(ii) Broad health benefits: antioxidant and anti-cancer properties	(ii) GuNP-gallic acid, taxifolin, hesperetin, quercetin, rutin				(ii)32/—	(ii) –OH, C–N, O–H, C≡N, C–H, C=O
	(iii) Holy basil (TNP)	(iii) Facilitates surface functionalization of CNPs and excellent radical scavenging	(iii) TNP-luteolin, apigenin, caffeic acid, rosmarinic acid, quercetin				(iii)42/—	(iii) O–H, C–O, C≡N C≡C, N=C=O
	(iv) Syzygium cumini (JNP)	(iv) Strong oxidant properties	(iv) JNP-quercetin, myricetin, maslinic acid, triacontanol				(iv) 23.5/—	(iv) C=O, O–H, C–N C–O C–H (v) C=O N–H, C=N

system.[101–103] Hence, a unified theory elucidating for the excitation dependent PL signal has been difficult to establish.[104] The largely accepted fluorescence mechanisms (schematic representation in Fig. 5) are briefly discussed below.

5.1 Quantum confinement effect (QCE)/size effect

Many theoretical researches have correlated the excitation-dependent emission with the quantum confinement in CDs, just as for metal-based quantum dots.[105] Close to Fermi level, a splitting of energy level occurs, wherein the electronic quasi continuous energy levels get transformed into distinct energy levels leading to widening of energy gap.[106] According to this phenomenon, when the particle size is brought down to nanometer dimensions, the PL emission is governed by the particle size. In effect, the "core size"/sp^2 domain size (the effective conjugated length) is the key factor, rather than the actual particle size.[107,108] An increase in "size" leads to a reduction in band gap, thus shifting the emission wavelength towards red. According to abstract modeling, some of the transitions (π–π^*) of sp^2 clusters lead to the radiative recombination of the excitons within the core, thus affecting the PL of CDs.[109,110]

5.2 Surface states

Sun *et al.* were the first to suggest that photoluminescence could be influenced by the surface states in CDs.[103] Since then, many researchers have supported the relation between the surface states and the functional groups present on the CDs' surface (–COOH, $-NH_2$, C=O, C=N, –OH, *etc.*). These groups bring in energy levels (fluorophores) within the energy gap which act as surface energy traps between π and π^* of the C–C band. Consequently, this surface modification/passivation with different functional groups eliminates various non-radiative electron–hole recombination centres, stabilizes CDs, and thus enhances their luminescence.[111]

Consequently, the electron transitions from these levels result in a red-shifted emission. Thus, by regulating the surface functional groups (heteroatomic doping), the PL emission behavior can be tailored.[112] The red-shifted PL emission in CDs is also influenced by the oxygen content present on their surface. The greater the extent of surface oxidation, the higher the proportion of surface defect sites on CDs.[113] These defects have the ability to capture excitons, the resulting radiation from the recombination of these trapped excitons causes a shift in PL emission towards red leading to a narrower energy band gap (surface-state-related emission).

The excitation dependent emission in most of the biomass-synthesised CDs has been ascribed to be due to different particle sizes (quantum effect) as well as the distributed emissive states, associated with various functional groups, present on CDs' surface. This may be attributed to the discrepancy in the compound structures present in the natural precursors, leading to a molecular transition mode change under different excitations, thus resulting in deviation in emission wavelength.[114] For example, the green luminescence of the CDs prepared from neem leaves has been attributed to surface energy traps.[64] However, amine functionalized CDs, (obtained by hydrothermally treating the CDs in ammonia), caused less accumulation resulting in a blue shift in PL emission in contrast to the originally observed green fluorescence. Some of the functional groups present on surface, like –COOH and epoxy, get substituted by $-CONH_2$ and $-C-NH_2$ after amine functionalization, which represses the non-radiative recombination in the intrinsic states, leading to a twofold magnification in the PL intensity.

5.3 Molecular state

In the process of synthesizing CDs *via* bottom-up approach, numerous molecular species (molecular fluorophores with conjugated carbons) are generated. These impurities, either free or attached to CDs' surface, regulate the fluorescence emission, thus influence its overall optical properties[115]

6. Detection of heavy metal ions and organic pollutants from IKS-based biomass precursors

The main work describing sensing of organic pollutants and heavy metal ions through IKS based green precursors are highlighted in Table 2. The table incorporates various IKS based natural precursors used in the synthesis of carbon-based sensors as an electrochemical/fluorescent/ratiometric/colorimetric nanoprobes to detect toxic contaminants. Some of the main characteristics used for the assessment of the CDs are quantum yield (QY), linear concentration range (LCR), and limit of detection (LOD), which demonstrate the overall efficiency of the biomass synthesised CDs towards the sensing of the analyte. Additionally, recovery and relative standard deviation observed in the presence of real samples have also been highlighted.

In a specific study conducted with Jackfruit seeds[95] as a biomass precursor to synthesize N-doped CDs *via* microwave-assisted method, *O*-phosphoric acid (mild acid) was added to enhance the absorption of microwave radiation that led to passivation of the surface. On the other hand, as an example of multimode detection approaches, in Giloy stem based CDs,[46] the authors also developed a smartphone-based sensing of the Congo red (CR) dye, apart from the colorimetric and fluorescence techniques, with high-definition images accompanied by the linear relationship of CR with color intensity. In another study, researchers produced hybrid CDs (h-CDs) from the leaves of *Tamarindus indica* and *Mangifera indica*[51] to develop ratiometric fluorescence sensor. The authors studied the color change of the PL intensity ratio of the h-CDs (obtained from blue (b) and green (g) emitting CDs) with the addition of Hg(II), the volume ratio of the two CDs and the duration of microwave irradiation. The Hg(II) detection sensitivity was observed highest for 2 : 1 ratio of b-CDs to g-CDs with microwave irradiation time of 15 minutes.[51]

Furthermore, in a detailed adsorption study with teak leaves biomass carbon dots (TBCDs), the authors evaluated efficiency of the CDs with MB dye and concluded the formation of an adduct between the two, which possessed a significant

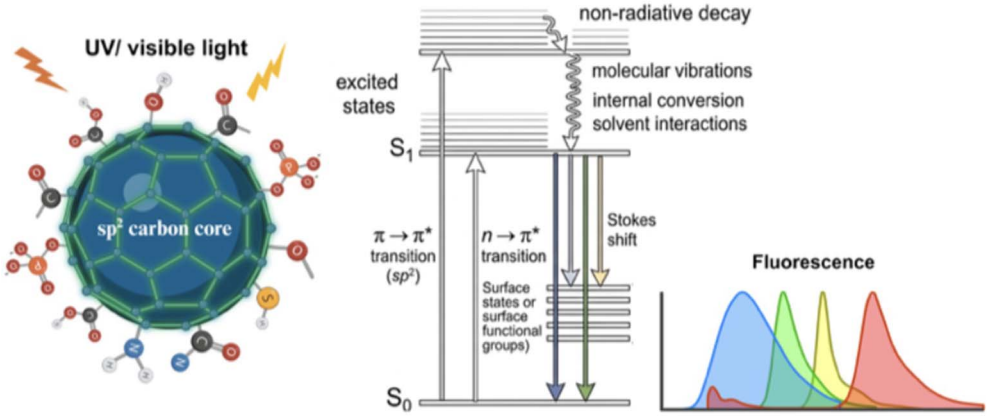

Fig. 5 Schematic representation of proposed photoluminescence mechanism in carbon dots.

adsorption capacity of 735.2 mg g^{-1} and removal efficiency of 50.1%. The 77.1% of the adsorbent's efficiency was restored after regeneration, making them effective for reuse.[71]

Using extracts of the bamboo leaves as the natural biomass material, two different types of multi-emission CD hybrids (dual-emission and three-emission CDs) were synthesised by solvothermal means under neutral and alkaline mediums, respectively. Further, these were employed as different ratiometric fluorescent nanosensors for the detection of Pb(II) and Hg(II), under ideal and real (river water) samples. The authors observed that the dual-emission CD (for the detection of Pb(II)), exhibited a linear positive correlation of I_{653}/I_{493} with increasing Pb(II) concentration, while for the three-emission nanosensor, the ratio I_{611}/I_{491} decreased linearly with increasing Hg(II) concentration, in artificial water samples. This indicated categorical Pb(II) and Hg(II) level-dependent ratiometric responses for both the CDs. The results confirmed that the ratiometric fluorescent nanosensors not only possessed exceptional sensitivity, selectivity and high precision, but also displayed built-in correction of external effects.[89]

For finding an ideal environment for the detection of Cr(VI) using jasmine leaves[75] synthesised CDs, the authors studied different factors like concentration of ions, pH, temperature, reaction time, and interfering species. The authors deduced the optimum pH for CDs-MnO_2 and NCDs-MnO_2 nanocomposites as 4 and 6 respectively, revealing requirement of more acidic environment for CDs-MnO_2. Further, the optimum reaction temperature and time interval for CDs-MnO_2 & NCDs-MnO_2 nanocomposites required for Cr(VI) detection was 65 °C & 45 °C and 4 min & 7 min, respectively. Further, both the nanocomposites exhibited interference with nitrate ions. Finally, they found NCDs-MnO_2 nanocomposite to be a better sensor of Cr(VI), attributing to its smaller size and the effective surface functional groups present.

The fluorescence quenching mechanism in tulsi leaves derived CDs for the detection of Cr(VI) was explained to be due to IFE. The authors demonstrated (three times), a significant recovery of the fluorescence by the addition of ascorbic acid which was ascribed to be due to the conversion of Cr(VI) to Cr(III), allowing the system to be recycled. Further, these CDs were used to sense Cr(VI) in real water samples (industrial water) with satisfactory results.[74] As another example, nitrogen doped CDs synthesised hydrothermally from betel leaves acted as a single probe system for dual sensing (picric acid, PA and Fe(III)) with remarkable sensitivity and selectivity. The fluorescence in these CDs displayed great stability even at high ionic strengths. The fluorescence quenching and the red shift (slight) of the emission spectrum with increasing PA concentration was explained to be due to the electrostatic interaction between the O & N based groups (CDs) and the phenolic group of analytes (PA). Likewise, the quenching observed with Fe(III) was explained to be due to chelation formation, leading to electron transfer from excited state of N-CDs to d-orbital (partially filled). This facilitated non-radiative recombination of electrons & holes, thus diminishing the fluorescence.

The N-CDs synthesised from *Ziziphus mauritiana*, were employed as a catalyst for the removal of Safranin-O (SO) dye, with $NaBH_4$ being used as a reducing agent. The authors achieved 79% degradation efficiency of the dye using N-CDs (at pH 12) in 18 minutes as compared to 48% (210 min) with $NaBH_4$ only. This was ascribed to the transfer of electrons from BH_4^- ions to the dye, with N-CDs acting as mediators.[78] In another study, reduction of SO dye was acheived by nitrogen doped CDs derived from neem seeds, which showed a 100% reduction in 6 minutes as compared to 28 minutes in undoped CDs.[50] Dwarf banana peel[84] synthesised CDs (doped with aqueous ammonia) as well as betel leaves[49] derived-NCDs can also be used as an invisible ink, in anticounterfeiting applications.

7. Underlying mechanisms for CDs-based optical sensors

In general, an interaction between CDs and analytes (organic/inorganic) results in spectral shift (blue/red/null) accompanied by either quenching or enhancement of their fluorescence intensity. This principle forms the basis for employing CDs as a sensor for detecting these analytes. Depending on the interactions between the CDs and the analytes, the quenching mechanism could be either, (i) static quenching (SQ) or

Table 2 Plant biomass used as precursors for optical sensing of heavy metal ions and organic pollutants[a]

S. no.	Precursor/dopant	Maximum PL emission wavelength, λ_{max}, (excitation wavelength, λ_{ex})/QYs	Analyte	Detection type/ degradation approach	Selectivity/sensitivity	Repeatability/recovery	Relative standard deviation (RSD)
01	Curry leaves extract and gold NPs (AuNPs) electrode on graphite sheet substrate[3,26]	—	Heavy metal ions: (i) Pb(II) (ii) Hg(II)	Electrochemical sensing	Pb(II), Hg(II)	—	—
02	Giloy stem/N, S doping[28,46]	520 nm (430 nm)/7.2%	Nitrophenol and dye: (i) 4-NP; (ii) CR	(i) Fluorometric quenching: IFE; LOD: 380 nM	(i) 3-NP, 4-NP, 2-NP, phenol, 1-naphthol, P-BQ, P-PDA, CNB, and biomolecules	(i) 4-NP (a) for tap water: —/94.67 to 103.45% (b) for pond water: —/93.88 to 102.49%	(i) 4-NP (a) for tap water: ≤3.96% ($n = 3$) (b) for pond water ≤4.38% ($n = 3$)
				(ii) Fluorometric quenching: IFE; colorimetric and smartphone techniques; LOD: 62 nM	(ii) CR, Ba(II), Ca(II), Cd(II), Cu(II), Mg(II), Mn(II), Na(I), K(I), Zn(II), Cl^-, NO_3^-, dyes, molecules (MB, aniline, MG, naphthol)	(ii) CR (a) for tap water: —/95.61 to 99.34% (b) for pond water: —/95.05 to 96.4%	(ii) CR (a) for tap water, ≤4.92 (b) for pond water 4.54% ($n = 3$)
03	"Shatavari" *Asparagus racemosus* root[27,48]	447 nm (216 nm)/—	Heavy metal ion: Ag(I)	Colorimetric: (i) CD color change from yellow to brown due to interactions between CDs and Ag(I); (ii) change in the maximum absorption wavelength (370 nm to 454 nm)	Ag(I), K(I), Na(I), Ca(II), Cd(II), Pb(II), Zn(II), Hg(II), Mg(II), As(V)	—	—
04	(i) Neem seed/aqueous NH_3 (as N source)[50,63]	400 nm (320 nm)/—	Dye: Safranin-O	Reduction of dye with $NaBH_4$ using CDs (6 min)	Safranin-O dye	—	—
05	Neem leaves + ammonia solution amine-terminated GQDs (Am-GQDs)[30,64]	—/2%	Heavy metal ion: Ag(I)	Fluorometric quenching original fluorescence regenerated using L-cysteine. LOD: 0.033–0.1 g L^{-1}	Ag(I), Ni(II), Cu(II), Co(II), Fe(II), Hg(II), Fe(III), Pb(II) can quench the fluorescence (off-state), only Ag(I) allows for the fluorescence recovery (on-state) upon L-cysteine addition	—	—
06	Jamun leaves[4,65] (O & N groups derived from phytochemicals)	460 nm (330 nm)/15.9%	Heavy metal ion: Fe(III)	Fluorometric quenching LOD: 0.13 μM LCR: 0–80 μM	Fe(III), Na(I), Mg(II), K(I), Pb(II), Ca(II), Mn(II), Zn(II), Cu(II), Cd(II), Ni(II), Co(II), Ba(II), Al(III), Cr(III)	—/88 to 106.5%	0.649 to 1.272%
07	Jamun fruit[66]	438 nm (350 nm)/5.9%	Heavy metal ion: Fe(III)	Fluorometric quenching and absorbance LOD: 0.001 μM LCR: 0.01–100 μM	Fe(III), Mg(II), K(I),Ca(II), Hg(II), Mn(II), Fe(II), Co(II), Pb(II), Zn(II), Ba(II), Cr(III), Al(III)	—/94.0 to 107.3%	0.03 to 1.63%

Table 2 (*Contd.*)

S. no.	Precursor/dopant	Maximum PL emission wavelength, λ_{max}, (excitation wavelength, λ_{ex})/QYs	Analyte	Detection type/ degradation approach	Selectivity/sensitivity	Repeatability/recovery	Relative standard deviation (RSD)
08	Pinewood[32,67]	447 nm (330 nm)/4.69%	Heavy metal ion: Fe(III)	Fluorometric LOD: 355.4 nM L^{-1} LCR: 0–1000 μM L^{-1} and 1000–2000 μM L^{-1}	Fe(III), K(I), Cd(II), Fe(II), Ag(I), Mg(II), Zn(II), Mn(II), Sn(II), Hg(II), Pb(II), Cu(II)	—	—
09	Pine needles/natural C & N source[47]	400 nm (320 nm)/7.65%	Heavy metal ion and food additives: (i) Fe(III) (ii) folic acid (FA)	Dual-mode: fluorometric and UV-Vis absorbance (i) Fe(III) LOD-0.04 μM (UV-Vis mode); 0.02 μM for the fluorescence mode) LCR: 0.1–540 μM; (ii) folic acid LOD-0.04 μM (fluorescence mode) 0.03 μM (UV-Vis mode); LCR: 0.1–165 μM	(i) Fe(III), Cd(II), Na(I), Mg(II), Ba(II), Ni(II), Cu(II), Li(I), Hg(II), Pb(II), K(I), Co(II), Ca(II), Zn(II), Fe(II) (ii) L-glutathione (GSH), L-cysteine (cys), glucose (glu), dopamine (DA), DL-homocysteine (Hcy), nicotinic acid (NA), ascorbic acid (AA), taurine (TA)	(i) For Fe –/98.66 to 102.46% (ii) For FA –/96.00 to 102.00%	(i) ≤ 1.78%. (ii) 1.95%
10	Pinecones (PC) and pine bark[5] (PB)	PCCD: 430 nm (360 nm)/11.3% PBCD: 430 nm (345 nm)/5.64%	Antibiotics: (i) tetracycline (TC) (ii) amoxicillin (AMX)	Fluorometric quenching: IFE (TC); SQ(AMX); (a) LOD for TC 0.062 μM for PCCDs (b) 0.2237 μM for PBCDs (ii) AMX LOD: 0.49 μM for PBCDs LCR: 5–100 μM	Amoxicillin (AMX), tetracycline (TC), Zn(II), Fe(III), Cd(II), Fe(II), Hg(II), Ni(II), chloramphenicol (CLM), ciprofloxacin (CIP), sulfamethazole (SMZ)	(i)TC —/96.12 to 102.74% (ii) AMX —/98.72 to 100.84%	(i) TC <2% (ii) AMX <1%
11	Tamarind leaves[33,51] blue emitting CQDs (b-CQD) & mango leaves green emitting CQDs (g-CQD) both CQDS combined to form hybrid CQDs (h-CQDs)	b-CQDs – blue emission/365 nm g-CQDs – green emission/365 nm	Heavy metal ion: Hg(II)	Ratiometric fluorescence	—	—	—
12	Tamarind shell waste[68] CQDs/ZnO nanocomposite	—	Dyes: MB, MG	Dye degradation with CDs-ZnO under solar light exposure. 100%/60 min	—	—	—
13	Lotus root[35,69]/nitrogen content of 5.23%	435 nm (360 nm)/19%	Heavy metal ion: Hg(II)	Fluorometric quenching; SQ/PET; LOD: 18.7 nM; LCR: 0.1 to 60.0 μM	Hg(II), Mg(II) Cd(II), Cu(II), Pb(II), Sr(II), Fe(III), Ca(II), Al(III), Ba(II), Co(II), Fe(II), Zn(II)	—/90.0 to 98.5%	—
14	Teak leaves[71]	—	Dye: MB	Adsorption of MB onto CDs (adduct formed between MB^+ dye and	—	Yes	—

Table 2 (*Contd.*)

S. no.	Precursor/dopant	Maximum PL emission wavelength, λ_{max}, (excitation wavelength, λ_{ex})/QYs	Analyte	Detection type/ degradation approach	Selectivity/sensitivity	Repeatability/recovery	Relative standard deviation (RSD)
				TBCDs$^-$) removal rate – 50.1%			
15	Tulsi leaves[72]	500 nm (450 nm)/9.3%	Heavy metal ion: Pb(II)	Fluorometric quenching: Pb(II) LOD: 0.59 nM; LCR: 0.01–1.0 μ M	Pb(II), Ni(II), Co(II), Cu(II), Cd(II), Hg(II), Ca(II), Mg(II), Sn(II), Na(I), K(I), Al(III)	—	—
16	Tulsi leaves[6]	405 nm (320 nm)/11.5%	Food additive: MG	Fluorometric quenching: both SQ and DQ: LOD 18 nM; LCR: 0.018–0.063 μM	—	—	—
17	Tulsi leaves[74]	435 nm (360 nm)/3.06%	Heavy metal ion: Cr(VI)	Fluorometric quenching: IFE + SQ; LOD: 4.5 ppb; LCR: 1.6–50 μM	Cr(VI), I^-, NO_3^-, $H_2PO_4^-$, HSO_4^-, Br^-, Cl^-, F^-, SO_4^-, CN^-, CH_3COO^-, IO_4^-/yes, can be used multiple times	—/93 to 99%	
18	Lily jasmine (aq. NH_3 as N dopant)[75,76] (i) (CDs-MnO_2) (ii) (NCDs-MnO_2)		Heavy metal ion: Cr(VI)	UV-Vis spectrophotometric method (i) for (CDs-MnO_2), LOD: 16 μM LCR:1–30 μM (ii) for (NCDs-MnO_2) LOD: 69 μM LCR: 7200 μM	Cr(VI), Hg(II), Co(II), Cu(II), Fe(III), OH^-, Cl^-, NO_3^-, SO_4^{2-}	(i) —/100.01 to 100.2% (ii) —/99.9 to 100.01%	
19	"Indian jujube" *Ziziphus mauritiana* fruit)[77,78]/aq. ammonia (N-CDs)	547 nm (370 nm)/—	Dye: safra nin-O (under the presence of $NaBH_4$)	N-CDs as catalyst for dye removal: removal efficiency −79% (18 min)	—	—	—
20	*Ziziphus mauritiana* pulp extract[79]/nitrogen-doped (N groups derived from phytochemicals)	450 nm (340 nm)/30%	Antibiotics: CIP	Fluorometric enhancement: PL enhancement attributed to complex formed between the amine group (CDs) and the carboxylate group (CIP) LOD: 0.56 μM LCR: 10–100 μM	Ciprofloxacin (CIP), gentamicin, ampicillin, amoxicillin, tetra-cycline, moxifloxacin, levofloxacin, and norfloxacin	—/92.7 to 101.50%	0.48 to 5.68%
21	Mango peels[80] (composite of CDs with molecularly imprinted polymers; CQDs@MIPs)	453 nm (360 nm)/—	Pesticide: mesotrione	Fluorometric quenching: SQ and electron transfer LOD: 4.7 nM L^{-1} LCR: 0.015 to 3.0 μM L^{-1}	Vitamin B5, vitamin B2, Zn(II), Ca(II), Fe(III), Na(I), Mg(II), K(I) leucine, glutamate, histidine, alanine, valine, glycine, isoleucine, arginine,	—/91.4 to 96.2%	3.2 to 6.1%

Table 2 (*Contd.*)

S. no.	Precursor/dopant	Maximum PL emission wavelength, λ_{max}, (excitation wavelength, λ_{ex})/QYs	Analyte	Detection type/ degradation approach	Selectivity/sensitivity	Repeatability/recovery	Relative standard deviation (RSD)
					threonine, aspartate, phenylalanine, proline, tryptophan, serine, methionine, tyrosine, lysine, fructose, glucose sucrose		
22	Bael patra fruit[82] (i) C-CDs (peel, hard shell) (ii) P-CDs (edible pulp) (iii) M-CDs (mixture of pulp and gum)	(i) 431 nm(330 nm)/ 17.39% (ii) 433 nm (350 nm)/ 59.07% (iii) 449 nm(370 nm)/ 55.25%	Food additive and heavy metal ion: (a) Allura red; (b) Fe(III)	Fluorometric quenching: DQ LOD for: (a) Allura red (i) 0.607 μM, (ii) 0.260 μM (iii) 0.166 μM LCR-0–30 μM (b) Fe(III) (i) 0.144 μM (ii) 0.142 μM (iii) 0.164 μM LCR: 0–150 μM	(i) Allura red, Congo red, erythrosine extra bluish, trypan blue, amaranth, Nile red, bromophenol blue, Sudan I, (ii) Fe(III), Ag(II), Ba(II), Bi(II), Co(II), Cu(II), Hg(I) K(I), Li(I), Mg(II), Ni(I), Pb(II), Ca(II), Cd(II) and different L-amino acids *i.e.* aspartic acid, asparagine, glutamine, tyrosine, leucine, isoleucine, histidine, alanine, arginine, cysteine, glutamic acid, valine and glycine lysine, methionine, phenylalanine, proline, serine, threonine, tryptophan	—/89.41 to 96.83%	—
23	(i) Dwarf banana peel[84]/ (+aq. NH_3)	413 nm (345 nm)/23%	Heavy metal ion: Fe(III)	Fluorometric quenching: Electron/ energy transfer (ET) between Fe(III) and HN-CDs (non-radiative) LOD-0.66 μM; LCR-5–25 μM	Fe(III), Ca(II), Al(III), Cd(II), Cr(III), Co(II), Cu(II), Mn(II) Hg(II), Zn(II), Pb(II), Ni(II)	—	—
24	Pseudo-stem of banana[86]	—/48%	Heavy metal ion Fe(III) and $S_2O_3^{2-}$	Fluorometric quenching: DQ (electron transfer from CDs to Fe(III)) (i) for Fe(III): LOD 6.4 nM; LCR 0–100 μM (ii) for $S_2O_3^{2-}$ LOD 0.847 μM	Fe(III), $S_2O_3^{2-}$, Ag(I), Co(II), Mn(II), Fe(II), Cr(III), Cu(II), Al(III), Pb(II), Mg(II), Ni(II), Zn(II), Hg(II), Ca(II), Cd(II), "turn-on" property towards $S_2O_3^{2-}$ anion	—	—

Table 2 (*Contd.*)

S. no.	Precursor/dopant	Maximum PL emission wavelength, λ_{max}, (excitation wavelength, λ_{ex})/QYs	Analyte	Detection type/ degradation approach	Selectivity/sensitivity	Repeatability/recovery	Relative standard deviation (RSD)
25	(i) Ripe banana peels[87] (BCD_{BP}) + ethylene diamine + L-cysteine	(i)437 nm (330 nm)/27%	Heavy metal ions (i) Fe(III) (ii) Cr(VI) (iii) dyes: MB, MG, MO and RB	Fluorometric quenching: (i) LOD: 121 pM LCR: 10–200 pM (ii)	(i) Fe(III), Cr(VI), Mg(II), Cu(II), Na(I), K(I), Hg(II), Cd(II)	(i) –/94.5 to 100.26%	(i) 0.30–1.45
	(ii) Dried rose petals (BCD_{RP}) + ethylene diamine + L-cysteine	(ii) 407 nm (316 nm)/ 28%		LOD: 81 pM LCR:10–100 pM (iii) adsorption for dye removal (>90% of dye removal)	(ii) Fe(III), Cr(VI), Hg(II), Mg(II), Cu(II), Na(I), Cd(II), K(I)	(ii) –/87.0 to 102.3%	(ii) 0.27–1.23
	(iii) Biochar				(iii) —	(iii)—	(iii)—
26	Betel leaves[49] N-doped CDs (betel leaves acted as C & N source)	428 nm (360 nm)/12%	Heavy metal ion: Fe(III)	Fluorometric quenching; resonance energy/electron transfer (RET) mechanism resulting in CDs + Fe(III) adduct LOD 0.43 μM, LCR 5–30 μm	(i) Fe(III), Al(III), Cd(II), Ca(II), Co(II), Cu(II), Cr(III), Hg(II), Ni(II), Mn(II), Zn(II), Pb(II)	—	—
27	Betel leaves[116] +ammonia solution (green N-dopant)	402 nm (320 nm)/4.21%	(i) Food additive: Picric acid (PA)	Enhancement in absorbance & Fluorometric quenching; (i) for PA LOD-0.11 μM LCR: 0.3–3.3 μM (ii) for Fe(III)	(i) Picric acid phenol, nitrobenzene, aniline, hydroquinone, 4-nitrophenol, benzo-quinone, benzoic acid, toluene	—	—
			(ii) Heavy metal ion Fe(III)	LOD: 0.135 μM; LCR: 0.3–3.3 μM	(ii) Fe(III), K(I), Cu(I), Na(I), Pb(II), Cu(II), Cr(VI), Zn(II), Fe(II), Cd(II), Ag(II), Hg(II) Mn(II)		
28	Bamboo leaves + anhydrous ethanol[89]	(i) 493 nm & 653 nm (400 nm)/4.7%	Heavy metal ions: (i) Pb(II); (ii) Hg(II)	Ratiometric fluorescence (i) for Pb(II): LOD: 0.14 nM; LCR: 0.6–800 nM (ii) for Hg(II): LOD: 0.22 nM; LCR: 1–1000 nM	(i) Pb(II) Al(III), Cr(III), Fe(III), Cu(II), Mg(II), Zn(II),Hg(II), Ca(II), Mn(II), Cd(II), Co(II), Ag(I), K(I),Na(I)	(i) –/91.4 to 105.6%	(i) 1.4 to 5.7% ($n = 6$)
	(i) Dual-emission CD nanohybrids	(ii) 491 nm, 611 nm, 665 nm (400 nm)/3.8%			(ii) Hg(II), Al(III), Pb(II) Fe(III), Cu(II), Cr(III), Mg(II), Ca(II), Zn(II), Cd(II), Mn(II), Ag(I), Co(II), K(I),Na(I)	(ii) 95.3 to 105%	(ii) 4.1–6.9% ($n = 6$)
	(ii) three-emission CD nanohybrids obtained with Na_2CO_3 solution						
29	Bamboo leaves[91] branched polyethylenimine (BPEI)-capped CQDs (BPEI-CQDs)	440 nm (365 nm)/7.1%	Heavy metal ion: Cu(II)	Fluorometric quenching: IFE; LOD: 115 nM; LCR: 0.333 to 66.6 M	Cu(II), Co(II), Mn(II), Ca(II), Ni(II), Hg(II), Cd(II) Pb(II),Ba(II)	—	—

Table 2 (*Contd.*)

S. no.	Precursor/dopant	Maximum PL emission wavelength, λ_{max}, (excitation wavelength, λ_{ex})/QYs	Analyte	Detection type/ degradation approach	Selectivity/sensitivity	Repeatability/recovery	Relative standard deviation (RSD)
30	Pomegranate juice[93] + ammonium hydroxide (as the nitrogen doping agent)	395 nm(310 nm)/—	Nanoparticles: Silver nanoparticles (AgNPs)	Fluorometric quenching: IFE; LOD: 3.8×10^{-10} M; LCR: 8.3×10^{-10} – 3.3×10^{-8} M	AgNPs, Ag(I), Fe(II), Al(III), Na(I), Mg(II), Ni(II), Cu(II) Zn(II)	—/96 to 105%	3.3–4.3%
31	Jackfruit seeds[95]	437 nm (360 nm)/ 17.91%	Heavy metal ion: Au(III)	Fluorometric quenching: (ground state complex formation) LOD: 239 nM; LCR: 0–100 μM	Na(I), K(I),Ca(II), Mn(II), Fe(II), Fe(III), Co(II), Cu(II), Zn(II), Ag(I), Hg(II), Pb(II), Au(III)	—	—
32	Gum Ghatti[97] C_{ZnO}-dots (CZ-2) Zn supported carbon dots	465 nm(370 nm)/—	Dye: MG	Photo-catalytic activity of the C_{ZnO}-dots (CZ-2). Degradation efficiency = 98.4%/60 min	—	3 times/—	
33	Turmeric powder[99]/ $CoFe_2O_4$; $CoFe_2O_4$-CD nanocomposite	565 nm (330 nm)/20%	Azo dyes: (i) acid black 24 (ii) acid Brown 14 (iii) acid red	Photo-catalytic activity of the $CoFe_2O_4$-CD nanocomposite	—	—	—
34	(i) Azadirachta indica (NNP)[100] (ii) Psidium guajava (GuNP) (iii) Holy basil (TNP) (iv) Syzygium cumini (JNP)	(i) —/21% (ii) —/17.8% (iii) —/25.2% (iv) —/19.3%	Heavy metal ions: (i) Fe(II) (ii) Ni(II) (iii) Fe(II) Pd(II) (iv) Fe(III)	Fluorescence quenching (i) DQ, LOD: 0.11 ppm (ii) SQ + DQ, LOD: 0.09 ppm (iii) DQ, 0.011 ppm and 0.0225 ppm (iv) DQ, LOD: 0. 012 ppm)	(i) Fe(II), K(I), Pb(II), Cu(II), Ni(II), Zn(II), CO(II), Ca(II), Fe(III), Mg(II), Sr(II) Al(III), (ii) Ni(II) K(I), Pb(II), Cu(II), Zn(II), CO(II), Ca(II), Mg(II), Fe(II), Fe(III), Al(III), Sr(II) (iii) Fe(II), Pb(II), K(I), Al(III), Cu(II), Ni(II), Zn(II), CO(II), Ca(II), Mg(II), Fe(III), Sr(II) (iv) Fe(III), K(I), Pb(II), Cu(II), Ni(II), Zn(II), CO(II), Ca(II), Mg(II), Fe(II), Fe(III), Al(III), Sr(II)	—	—

[a] Nitrophenol – NP, Congo red – CR, malachite green – MG, methylene blue – MB, Rhodamine B – RB, methyl orange – MO, ciprofloxacin – CIP.

dynamic quenching (DQ); (ii) Inner Filter Effect (IFE) or Foerster resonance energy transfer (FRET); (iii) Dexter energy transfer (DET) or Photoinduced electron transfer (PET) (Fig. 6).[117]

In static quenching (SQ), a weak bonding between the CDs (fluorophore) at ground state and the quencher results in the formation of a non-luminous complex. In contrast, dynamic quenching (DQ) results because of the collision between the CDs and the quencher molecules involving charge/energy transfer, which leads to the de-excitation of CDs and hence reduction in PL intensity.[118] However, there are few remarkable differences between the two phenomena: in SQ, the luminous lifetime of CDs remains the same (before and after being exposed to the quencher), whereas the absence/presence of quenchers in the detection system affects (shortens) PL lifetime in the case of DQ. In addition, for static quenching, the ground-state complex formation can cause observable changes in absorption spectrum of CDs (shift in peak position/increased number of UV absorption peaks *etc.*) while no change in absorption spectra is detected for DQ. Further, an increase in temperature minimizes the SQ effect, whereas vigorous collisions cause an escalation in DQ effect under high temperature conditions.

The IFE occurs when the UV-visible absorbance spectra of quenchers interfere or overlap spectrally with CDs' fluorescence (FL) excitation or emission spectra, which results in quenching of the PL intensity.[119] This effect eliminates any interaction between the CDs and the quencher. In most cases, IFE does not cause any variation in CD's absorption spectrum, implying that no new substance is being formed. Hence, the presence or absence of the quencher does not impact CD's average PL lifetime. Whereas in FRET, an overlap of the donors' (CD's) emission spectrum and the acceptor's (quencher's) absorption spectrum occurs, resulting in non-radiative energy transfer between CDs in the excited state and quencher in the ground state (involving dipole–dipole interaction between the two). This transfer is highly effective when the distance between the donor and the receptor is within 10 nm. Also, the PL lifetime of fluorophores (CDs) decreases after their interaction with quenchers in the case of FRET.[120]

The PET sensing mechanism involves formation of complex between CDs and the target analyte. Irradiation with light causes excitation of electrons in CDs. When the transfer of electrons occurs from activated CDs (electron donor) to the quenchers (electron receptor), the process is termed as oxidative PET. On the other hand, the electron transfer from the analyte/quencher (electron donor) to activated CDs (electron acceptor) is named as reductive PET. The deexcitation of electrons, causes non-radiative luminescence and thus changes the PL intensity.[120] DET is another process wherein a matching of the redox potentials of donors and acceptors is essential for the electron transfer to take place.

The CDs have also been employed in the photo induced degradation of organic dyes. In addition, CDs with metal oxides/semiconductors (composites) having vast surface area as well as exceptional absorption capacity, act as hybrid photocatalysts promoting e-h separation. This further expedites the transfer of electrons, escalating the reduction/oxidation capability of generated carriers, leading to enhanced photo decolorization[121,122]

The PL enhancement-based detection of Ciprofloxacin (CIP) from the green CDs synthesized from *Ziziphus mauritiana* pulp has been reported based on the complex formation between the

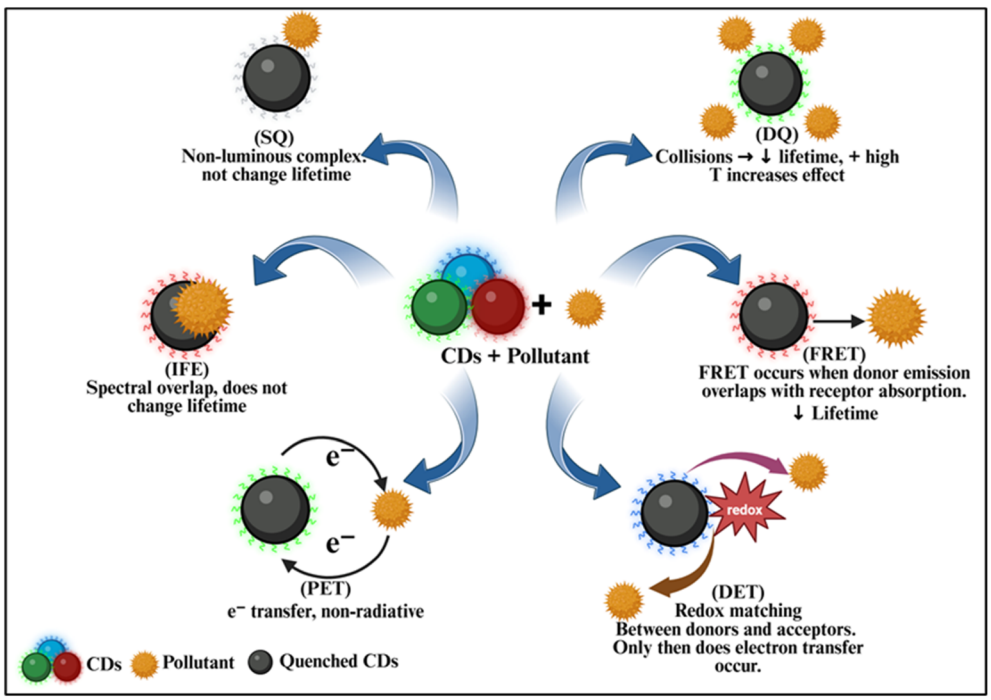

Fig. 6 Proposed detection mechanisms in CDs based optical sensors.

amine group from CDs and the carboxylate group of CIP.[79] The PL enhancement was attributed to several factors: (a) transfer of electrons from CDs to CIP; (b) interactions between the functional groups of the analyte and CDs through hydrogen bonding; (c) the reduction of surface defects of CDs' in the presence of CIP.

On the other hand, a colorimetric sensor is an elementary device used to assess an analyte by observing/measuring the color resolution (the depth of color)/change.[120] The mechanism responsible for the color change in carbon dot-based colorimetric sensor involves special interactions between carbon dots and the target analytes which impact CDs' optical properties. As an example, when $AgNO_3$ is exposed to CDs solution, the crucial interactions between the oxygen containing functional groups (hydroxyl, carboxyl and carbonyl), present on the surface of CDs help in enabling electron transfer efficiently to silver ions, leading to reduction of $AgNO_3$ to form silver nanoparticles (AgNPs) and thus act as sensors.[48]

Furthermore, designing of the ratiometric fluorescent probes is based on the relative change observed in fluorescence intensity of the emission peaks with the addition of analytes.[123] The ratio of the PL intensity at two different wavelengths is found to be directly proportional to the analyte concentration, thus helps in setting a coherent self-calibration system capable of eliminating false signals. Hence, this method is more accurate, sensitive as well as more resistant to environmental disturbances and instrumental settings. For example, to detect Hg(II) in pure and simulated seawater, ratiometric fluorescence assay between blue carbon quantum dots (b-CQDs) (produced from *Tamarindus indica* leaves) and green carbon quantum dots (g-CQDs) (produced from *Mangifera indica* leaves) was employed to synthesize hybrid carbon quantum dots (h-CQDs).[51] An increase in the PL intensity ratio was observed with increasing mercury ion concentration and hence it could be used to assess the change in color (blue to green) with the addition of Hg(II).

8. Summary and outlook

In conclusion, carbon dots and their composites synthesized using plants from Indian knowledge system represent a sustainable and versatile platform with promising applications in environmental remediation. The vast diversity of natural compounds (plant metabolites/phytochemicals) present in these plants provides a distinctive strength for tuning the properties of carbon dots. However, issues of repeatability/precision due to variability in biogenic substances, mechanistic understanding at molecular level, potential toxicity, and mass production remain among the main challenges to be addressed in the near future. The fundamental understanding of the connection between the phytochemicals present in the green precursor and the characteristics of the CDs after processing is necessary for the design and synthesis of predictable carbon-based nanomaterials. In addition, due to the vastness of IKS, integrating traditional plant-based resources with advanced approaches/techniques for developing standardized carbon dots synthesis protocols is also essential. Simultaneous evaluation of long-term ecological impacts is also crucial for creating large-scale, viable options. Through collaborative and systematic efforts from researchers in the field of biology, chemistry, materials science, medicine and engineering, plant-mediated carbon-based materials derived from India's vast biodiversity hold tremendous opportunity to advance the field of green nanotechnology and make significant to global sustainable development.

Conflicts of interest

There are no conflicts to declare.

Data availability

This review does not generate new data. The data used for analysis and discussion are derived from previously published studies, which are appropriately cited throughout the manuscript.

References

1 P. Pratim Sarma, K. Barman and P. K. Baruah, Green synthesis of silver nanoparticles using Murraya koenigii leaf extract with efficient catalytic, antimicrobial, and sensing properties towards heavy metal ions, *Inorg. Chem. Commun.*, 2023, **152**, 110676.
2 T. Gupta, K. Ansari, D. Lataye, M. Kadu, M. A. Khan, N. M. Mubarak, R. Garg and R. R. Karri, Adsorption of Indigo Carmine Dye by Acacia nilotica sawdust activated carbon in fixed bed column, *Sci. Rep.*, 2022, **12**, 15522.
3 N. Syakimah Ismail, A. Safiy Kamarul Ariffin, N. Izzati Akmal Mohd Azman, N. Hamidah Abdul Halim, N. Sabani, N. Juhari and S. Aisyah Shamsudin, Electrochemical Detection of Heavy Metal Ions using Gold Nanoparticles on Carbon Dots Extracted from Curry Leaves, *International Journal of Nanoelectronics and Materials*, 2024, 195–202.
4 Qurtulen, A. Ahmad, H. Salimi Shahraki, N. Khan, M. Ahmad and R. Bushra, One-pot synthesized fluorescent CDs from Syzygium cumini for metal ion sensing and cell imaging, *Inorg. Chem. Commun.*, 2024, **160**, 111883.
5 S. O. Sanni, A. A. Bayode, H. G. Brink, N. H. Haneklaus, L. Fu, J. Shang and H.-J. S. Fan, Green Carbon Dots from Pinecones and Pine Bark for Amoxicillin and Tetracycline Detection: A Circular Economy Approach, *J. Xenobiot.*, 2025, **15**, 43.
6 D. Shukla, F. P. Pandey, P. Kumari, N. Basu, M. K. Tiwari, J. Lahiri, R. N. Kharwar and A. S. Parmar, Label-Free Fluorometric Detection of Adulterant Malachite Green Using Carbon Dots Derived from the Medicinal Plant Source *Ocimum tenuiflorum*, *ChemistrySelect*, 2019, **4**, 4839–4847.
7 Y. Bian, Y. Zhang, Z. Chen, L. Xu, C. Zhang, D. Shi, X. Feng and X. Wang, Malachite green in environmental samples: Updates on sources, fates, distribution and removal techniques, *Ecotoxicol. Environ. Saf.*, 2025, **303**, 118978.

8 M. R. Gadekar and M. Mansoor Ahammed, Coagulation/floculation process for dye removal using water treatment residuals: modelling through artificial neural networks, *Desalin. Water Treat.*, 2016, **57**(55), 26392–26400.
9 S. Lim, J. L. Shi, U. von Gunten and D. L. McCurry, Ozonation of organic compounds in water and wastewater: A critical review, *Water Res.*, 2022, **213**, 118053.
10 A. Asghar, A. A. Abdul Raman and W. M. A. Wan Daud, Advanced oxidation processes for in-situ production of hydrogen peroxide/hydroxyl radical for textile wastewater treatment: a review, *J. Clean. Prod.*, 2015, **87**, 826–838.
11 I. Groeneveld, M. Kanelli, F. Ariese and M. R. van Bommel, Parameters that affect the photodegradation of dyes and pigments in solution and on substrate – An overview, *Dyes Pigm.*, 2023, **210**, 110999.
12 E.-Z. Tan, P.-G. Yin, T. You, H. Wang and L. Guo, Three Dimensional Design of Large-Scale TiO $_2$ Nanorods Scaffold Decorated by Silver Nanoparticles as SERS Sensor for Ultrasensitive Malachite Green Detection, *ACS Appl. Mater. Interfaces*, 2012, **4**, 3432–3437.
13 M.-C. Yang, J.-M. Fang, T.-F. Kuo, D.-M. Wang, Y.-L. Huang, L.-Y. Liu, P.-H. Chen and T.-H. Chang, Production of Antibodies for Selective Detection of Malachite Green and the Related Triphenylmethane Dyes in Fish and Fishpond Water, *J. Agric. Food Chem.*, 2007, **55**, 8851–8856.
14 W. Xing, L. He, H. Yang, C. Sun, D. Li, X. Yang, Y. Li and A. Deng, Development of a sensitive and group-specific polyclonal antibody-based enzyme-linked immunosorbent assay (ELISA) for detection of malachite green and leucomalachite green in water and fish samples, *J. Sci. Food Agric.*, 2009, **89**, 2165–2173.
15 M. Tholkappian, R. Ravisankar, A. Chandrasekaran, J. P. P. Jebakumar, K. V. Kanagasabapathy, M. V. R. Prasad and K. K. Satapathy, Assessing heavy metal toxicity in sediments of Chennai Coast of Tamil Nadu using Energy Dispersive X-Ray Fluorescence Spectroscopy (EDXRF) with statistical approach, *Toxicol Rep.*, 2018, **5**, 173–182.
16 T. A. Maryutina and N. S. Musina, Determination of metals in heavy oil residues by inductively coupled plasma atomic emission spectroscopy, *J. Anal. Chem.*, 2012, **67**, 862–867.
17 H. Wang, Z. Wu, B. Chen, M. He and B. Hu, Chip-based array magnetic solid phase microextraction on-line coupled with inductively coupled plasma mass spectrometry for the determination of trace heavy metals in cells, *Analyst*, 2015, **140**, 5619–5626.
18 Y. Safari, M. Karimaei, K. Sharafi, H. Arfaeinia, M. Moradi and N. Fattahi, Persistent sample circulation microextraction combined with graphite furnace atomic absorption spectroscopy for trace determination of heavy metals in fish species marketed in Kermanshah, Iran, and human health risk assessment, *J. Sci. Food Agric.*, 2018, **98**, 2915–2924.
19 L. Sun, C. Sun and X. Sun, Screening highly selective ionophores for heavy metal ion-selective electrodes and potentiometric sensors, *Electrochim. Acta*, 2016, **220**, 690–698.
20 A. Han, S. Hao, Y. Yang, X. Li, X. Luo, G. Fang, J. Liu and S. Wang, Perspective on recent developments of nanomaterial based fluorescent sensors: applications in safety and quality control of food and beverages, *J. Food Drug Anal.*, 2020, **28**, 487–508.
21 M. R. Willner and P. J. Vikesland, Nanomaterial enabled sensors for environmental contaminants, *J. Nanobiotechnol.*, 2018, **16**, 95.
22 S. D. Torres Landa, N. K. Reddy Bogireddy, I. Kaur, V. Batra and V. Agarwal, Heavy metal ion detection using green precursor derived carbon dots, *iScience*, 2022, **25**, 103816.
23 N. Sarma, *Environmental Awareness at the Time of Vedas*, Veda-Vidyā, 2015.
24 P. Ranjan, *Trivedi, Environmental Pollution and Control*, A. P. H. Publishing Corporation, New Delhi, 2004.
25 R. Renugadevi, Environmental ethics in the Hindu Vedas and Puranas in India, *Afr. J. Hist. Cult.*, 2012, **4**, 1–3.
26 L. A. Nigam, A Review on Medicinal Benefits of Curry Leaves, *J. Adv. Pharmacogn.*, 2023, **3**, 19–26.
27 N. Bopana and S. Saxena, Asparagus racemosus—Ethnopharmacological evaluation and conservation needs, *J. Ethnopharmacol.*, 2007, **110**, 1–15.
28 A. Gupta, H. Chandra Pant, N. Singh, N Saini, A. Mishra and H Tomar, *Adalya*, 2021, **10**, 57–67.
29 S. Drabu, S. Khatri and S. Babu, Neem: Healer of all ailments, *Res. J. Pharm., Biol. Chem. Sci.*, 2012, **3**, 120–126.
30 V. S. Kumar and V. Navaratnam, Neem (Azadirachta indica): Prehistory to contemporary medicinal uses to humankind, *Asian Pac. J. Trop. Biomed.*, 2013, **3**, 505–514.
31 T. Singh, P. Singh, V. K. Pandey, R. Singh and A. H. Dar, A literature review on bioactive properties of betel leaf (Piper betel L.) and its applications in food industry, *Food Chem. Adv.*, 2023, **3**, 100536.
32 B. Kanchan, B. Prerna and K. Simran, Medicinal Value of Secondary Metabolites of Pines grown in Himalayan Region of India, *Res. J. Biotechnol.*, 2020, **15**, 131–140.
33 N. Naeem, F. Nadeem, M. W. Azeem and R. M. Dharmadasa, Tamarindus indica–A review of explored potentials, *Int. J. Chem. Biochem. Sci.*, 2017, **12**, 98–106.
34 Y. M. Vispute, N. Thosar and P. Chavarkar, Bael Patra as Anti-Oxidant: A Review, *Int. J. Res. Appl. Sci. Eng. Technol.*, 2023, **11**, 743–750.
35 P. Ranchana, S. P. Thamaraiselvi, R. Baranidharan, R. Mangaiyarkarasi, M. Arunkumar, S. P. Mirunalini and K. Praiselin, Lotus (National Flower of India): A review on floral biology, ornamental, nutritional and medicinal importance, *Pharm. Innov. J.*, 2023, **12**, 2810–2818.
36 D. P. Nirala, A Review on Uses of Bamboo Including Ethno-Botanical Importance, *Int. J. Pure App. Biosci.*, 2017, **5**, 515–523.
37 B. Singh, P. Shankar, A. R. K. Mishra and H. Deupa, Potential of jackfruit seed as a functional ingredient: A Review, *Int. J. Agric. Food Sci.*, 2025, **7**, 283–289.
38 B. U. M. Enriquez, M. Rangel-Ayala, Y. Kumar, J. E. Garcia, J. F. Gomez-Aguilar, S. Khandual and V. Agarwal, Multifunctional Arthrospira platensis biomass derived

carbon dots: Sensing/removal of heavy metal ions, high-power light-emitting devices, and some machine learning assisted approaches for solid state sensor, *J. Environ. Chem. Eng.*, 2025, **13**, 117827.

39 B. U. M. Enriquez, M. Rangel, Y. Kumar, S. Khandual and V. Agarwal, Algae derived carbon dots and its polymeric composites for white light emission, *J. Lumin.*, 2025, **277**, 120955.

40 H. K. M. Ng, G. K. Lim and C. P. Leo, Comparison between hydrothermal and microwave-assisted synthesis of carbon dots from biowaste and chemical for heavy metal detection: A review, *Microchem. J.*, 2021, **165**, 106116.

41 M. B. Gawande, S. N. Shelke, R. Zboril and R. S. Varma, Microwave-Assisted Chemistry: Synthetic Applications for Rapid Assembly of Nanomaterials and Organics, *Acc. Chem. Res.*, 2014, **47**, 1338–1348.

42 N. K. R. Bogireddy, S. E. Sotelo Rios and V. Agarwal, Simple one step synthesis of dual-emissive heteroatom doped carbon dots for acetone sensing in commercial products and Cr (VI) reduction, *Chem. Eng. J.*, 2021, **414**, 128830.

43 R. Kumar, V. B. Kumar and A. Gedanken, Sonochemical synthesis of carbon dots, mechanism, effect of parameters, and catalytic, energy, biomedical and tissue engineering applications, *Ultrason. Sonochem.*, 2020, **64**, 105009.

44 H. Xu, B. W. Zeiger and K. S. Suslick, Sonochemical synthesis of nanomaterials, *Chem. Soc. Rev.*, 2013, **42**, 2555–2567.

45 R. Sha, S. S. Jones, N. Vishnu, B. Soundiraraju and S. Badhulika, A Novel Biomass Derived Carbon Quantum Dots for Highly Sensitive and Selective Detection of Hydrazine, *Electroanalysis*, 2018, **30**, 2228–2232.

46 S. Swain and A. K. Jena, Green Synthesis of N,S-Doped Carbon Dots from the Giloy Stem for Fluorimetry Detection of 4-Nitrophenol, Triple-Mode Detection of Congo Red, and Antioxidant Applications, *ACS Omega*, 2025, **10**, 5874–5885.

47 B. Wang, L. Guo, X. Yan, F. Hou, L. Zhong and H. Xu, Dual-mode detection sensor based on nitrogen-doped carbon dots from pine needles for the determination of Fe3+ and folic acid, *Spectrochim. Acta, Part A*, 2023, **285**, 121891.

48 P. Bijesh, V. Andal and V. Selvaraj, Microwave synthesis of carbon dot from asparagus racemosus for Ag+ ion sensing, anti-oxidant and cytotoxicity studies, *Bull. Chem. Soc. Ethiop.*, 2025, **39**, 907–920.

49 R. Atchudan, T. N. J. I. Edison, S. Perumal, R. Vinodh and Y. R. Lee, Betel-derived nitrogen-doped multicolor carbon dots for environmental and biological applications, *J. Mol. Liq.*, 2019, **296**, 111817.

50 C. Dhanush and M. G. Sethuraman, Influence of phyto-derived nitrogen doped carbon dots from the seeds of Azadirachta indica on the NaBH4 reduction of Safranin-O dye, *Diam. Relat. Mater.*, 2020, **108**, 107984.

51 R. C. Magnaye, R. B. De Castro, K. B. Gomez, G. M. Laylo and J. G. Maderazo, Synthesis of hybrid carbon quantum dots from tamarindus indica and mangifera indica leaves for the detection of mercury (Hg 2+) ion in purified water and simulated seawater (Sintesis Titik Kuantum Karbon Hibrid dari Daun Tamarindus indica dan Mangifera indica bagi Pengesanan Ion Merkuri (Hg 2+) dalam Sampel Air Tulen dan Simulasi Air Laut), *Malays. J. Anal. Sci.*, 2021, **25**(6), 1122–1137.

52 F. Rigodanza, M. Burian, F. Arcudi, L. Đorđević, H. Amenitsch and M. Prato, Snapshots into carbon dots formation through a combined spectroscopic approach, *Nat. Commun.*, 2021, **12**, 2640.

53 M. L. Liu, B. Bin Chen, C. M. Li and C. Z. Huang, Carbon dots: synthesis, formation mechanism, fluorescence origin and sensing applications, *Green Chem.*, 2019, **21**, 449–471.

54 T.-H. Chen and W.-L. Tseng, Self-Assembly of Monodisperse Carbon Dots into High-Brightness Nanoaggregates for Cellular Uptake Imaging and Iron(III) Sensing, *Anal. Chem.*, 2017, **89**, 11348–11356.

55 B. Bin Chen, R. S. Li, M. L. Liu, H. Z. Zhang and C. Z. Huang, Self-exothermic reaction prompted synthesis of single-layered graphene quantum dots at room temperature, *Chem. Commun.*, 2017, **53**, 4958–4961.

56 J. Kudr, L. Richtera, K. Xhaxhiu, D. Hynek, Z. Heger, O. Zitka and V. Adam, Carbon dots based FRET for the detection of DNA damage, *Biosens. Bioelectron.*, 2017, **92**, 133–139.

57 C. Yang, S. Zhu, Z. Li, Z. Li, C. Chen, L. Sun, W. Tang, R. Liu, Y. Sun and M. Yu, Nitrogen-doped carbon dots with excitation-independent long-wavelength emission produced by a room-temperature reaction, *Chem. Commun.*, 2016, **52**, 11912–11914.

58 Y. Su, M. Zhang, N. Zhou, M. Shao, C. Chi, P. Yuan and C. Zhao, Preparation of fluorescent N,P-doped carbon dots derived from adenosine 5′-monophosphate for use in multicolor bioimaging of adenocarcinomic human alveolar basal epithelial cells, *Microchim. Acta*, 2017, **184**, 699–706.

59 J. Cheng, C.-F. Wang, Y. Zhang, S. Yang and S. Chen, Zinc ion-doped carbon dots with strong yellow photoluminescence, *RSC Adv.*, 2016, **6**, 37189–37194.

60 D. Chao, J. Chen, Q. Dong, W. Wu, D. Qi and S. Dong, Ultrastable and ultrasensitive pH-switchable carbon dots with high quantum yield for water quality identification, glucose detection, and two starch-based solid-state fluorescence materials, *Nano Res.*, 2020, **13**, 3012–3018.

61 Y. Xu, X.-H. Jia, X.-B. Yin, X.-W. He and Y.-K. Zhang, Carbon Quantum Dot Stabilized Gadolinium Nanoprobe Prepared via a One-Pot Hydrothermal Approach for Magnetic Resonance and Fluorescence Dual-Modality Bioimaging, *Anal. Chem.*, 2014, **86**, 12122–12129.

62 Z. Song, F. Quan, Y. Xu, M. Liu, L. Cui and J. Liu, Multifunctional N,S co-doped carbon quantum dots with pH- and thermo-dependent switchable fluorescent properties and highly selective detection of glutathione, *Carbon*, 2016, **104**, 169–178.

63 E. Mondal and K. Chakraborty, Azadirachta indica - A Tree With Multifaceted Applications: An Overview, *J. Pharmaceut. Sci. Res.*, 2016, **8**, 299–306.

64 A. Suryawanshi, M. Biswal, D. Mhamane, R. Gokhale, S. Patil, D. Guin and S. Ogale, Large scale synthesis of graphene quantum dots (GQDs) from waste biomass and their use as an efficient and selective photoluminescence on–off–on probe for Ag^{+} ions, *Nanoscale*, 2014, **6**, 11664–11670.

65 A. B. M. N. Uddin, F. Hossain, A. S. M. A. Reza, M. S. Nasrin and A. H. M. K. Alam, Traditional uses, pharmacological activities, and phytochemical constituents of the genus *Syzygium* : A review, *Food Sci. Nutr.*, 2022, **10**, 1789–1819.

66 J. R. Bhamore, S. Jha, R. K. Singhal and S. K. Kailasa, Synthesis of Water Dispersible Fluorescent Carbon Nanocrystals from Syzygium cumini Fruits for the Detection of Fe3+ Ion in Water and Biological Samples and Imaging of Fusarium avenaceum Cells, *J. Fluoresc.*, 2017, **27**, 125–134.

67 S. Zhao, X. Song, X. Chai, P. Zhao, H. He and Z. Liu, Green production of fluorescent carbon quantum dots based on pine wood and its application in the detection of Fe3+, *J. Clean. Prod.*, 2020, **263**, 121561.

68 S. Shalini, T. Sasikala, D. Tharani, R. Venkatesh and S. Muthulingam, Novel green CQDs/ZnO binary photocatalyst synthesis for efficient visible light irradiation of organic dye degradation for environmental remediation, *J. Mol. Liq.*, 2024, **410**, 125525.

69 D. Gu, S. Shang, Q. Yu and J. Shen, Green synthesis of nitrogen-doped carbon dots from lotus root for Hg(II) ions detection and cell imaging, *Appl. Surf. Sci.*, 2016, **390**, 38–42.

70 R. B. Nidavani and A. M. Mahalakshmi, Teak (Tectona grandis Linn.): A renowned timber plant with potential medicinal values, *Int. J. Pharm. Pharmaceut. Sci.*, 2014, **6**, 48–54.

71 Z. W. Basha, A. S. Kumar and S. Muniraj, Green synthesis of carbon quantum dots from teak leaves biomass for in situ precipitation and regenerative-removal of methylene blue-dye, *Environ. Sci. Pollut. Res.*, 2024, **32**, 28143–28158.

72 A. Kumar, A. R. Chowdhuri, D. Laha, T. K. Mahto, P. Karmakar and S. K. Sahu, Green synthesis of carbon dots from Ocimum sanctum for effective fluorescent sensing of Pb2+ ions and live cell imaging, *Sens. Actuators, B*, 2017, **242**, 679–686.

73 S. Thakur, S. Choudhary and B. Walia, Tulsi - A Review Based Upon Its Ayurvedic and Modern Therapeutic Uses, *Int. J. Res. Rev.*, 2021, **8**, 263–272.

74 S. Bhatt, M. Bhatt, A. Kumar, G. Vyas, T. Gajaria and P. Paul, Green route for synthesis of multifunctional fluorescent carbon dots from Tulsi leaves and its application as Cr(VI) sensors, bio-imaging and patterning agents, *Colloids Surf., B*, 2018, **167**, 126–133.

75 T. Riaz, R. Azam, T. Shahzadi, S. Shahid, S. Mansoor, M. Javed, A. Bahadur, S. Iqbal, S. Mahmood, K. M. Alotaibi and M. Alshalwi, Carbon dots and nitrogen-doped carbon dots-metal oxide nanocomposites: robust agents for effective sensing of ions, *J. Mater. Sci.: Mater. Electron.*, 2024, **35**, 940.

76 D. Reshma, C. T. Anitha and S. T. Tharakan, Phytochemical and pharmacological properties of five different species of jasminum, *Plant Arch.*, 2021, **21**(2), 126–136.

77 M. Goyal, D. Sasmal and B. Nagori, Review on Ethnomedicinal uses, Pharmacological activity and Phytochemical constituents of & lt;i& gt;Ziziphus mauritiana& lt;/i& gt; (& lt;i& gt;Z. jujuba& lt;/i& gt; Lam., non Mill), *Spatula DD*, 2012, **2**, 107.

78 S. Rajapandi, S. Nangan, T. Natesan, A. Kumar, G. Dharman, M. Pandeeswaran, D. Verma, M. Ubaidullah, B. Pandit, N. Dhaliwal, S. S. Sehgal, R. Rangappan and G. N. Kousalya, Ziziphus mauritiana-derived nitrogen-doped biogenic carbon dots: Eco-friendly catalysts for dye degradation and antibacterial applications, *Chemosphere*, 2023, **338**, 139584.

79 N. Chaudhary, D. Verma, A. K. Yadav, J. G. Sharma and P. R. Solanki, Rational hydrothermal-assisted green synthesis of blueish emitting carbon dots as an optical sensing platform for antibiotic detection in the milk sample, *Talanta Open*, 2023, **8**, 100259.

80 X. Sun, Y. Liu, N. Niu and L. Chen, Synthesis of molecularly imprinted fluorescent probe based on biomass-derived carbon quantum dots for detection of mesotrione, *Anal. Bioanal. Chem.*, 2019, **411**, 5519–5530.

81 G. M. Masud Parvez, Pharmacological Activities of Mango (Mangifera Indica): A Review GM Masud Parvez, *J. Pharmacogn. Phytochem.*, 2016, **5**(3), 1–7.

82 A. Vijeata, S. Chaudhary and G. R. Chaudhary, Fluorescent carbon dots from Indian Bael patra as effective sensing tool to detect perilous food colorant, *Food Chem.*, 2022, **373**, 131492.

83 Y. M. Vispute, N. Thosar and P. Chavarkar, Bael Patra as Anti-Oxidant: A Review, *Int. J. Res. Appl. Sci. Eng. Technol.*, 2023, **11**, 743–750.

84 R. Atchudan, T. N. J. I. Edison, S. Perumal, N. Muthuchamy and Y. R. Lee, Hydrophilic nitrogen-doped carbon dots from biowaste using dwarf banana peel for environmental and biological applications, *Fuel*, 2020, **275**, 117821.

85 A. Yadav, Banana (Musa acuminata): Most popular and common Indian plant with multiple pharmacological potentials, *World J. Biol. Pharm. Health Sci.*, 2021, **7**, 036–044.

86 S. A. A. Vandarkuzhali, V. Jeyalakshmi, G. Sivaraman, S. Singaravadivel, K. R. Krishnamurthy and B. Viswanathan, Highly fluorescent carbon dots from Pseudo-stem of banana plant: Applications as nanosensor and bio-imaging agents, *Sens. Actuators, B*, 2017, **252**, 894–900.

87 M. Das, H. Thakkar, D. Patel and S. Thakore, Repurposing the domestic organic waste into green emissive carbon dots and carbonized adsorbent: A sustainable zero waste process for metal sensing and dye sequestration, *J. Environ. Chem. Eng.*, 2021, **9**, 106312.

88 T. Singh, P. Singh, V. K. Pandey, R. Singh and A. H. Dar, A literature review on bioactive properties of betel leaf (Piper betel L.) and its applications in food industry, *Food Chem. Adv.*, 2023, **3**, 100536.

89 Z. Liu, W. Jin, F. Wang, T. Li, J. Nie, W. Xiao, Q. Zhang and Y. Zhang, Ratiometric fluorescent sensing of Pb2+ and Hg2+ with two types of carbon dot nanohybrids synthesized from the same biomass, *Sens. Actuators, B*, 2019, **296**, 126698.

90 D. P. Nirala, A Review on Uses of Bamboo Including Ethno-Botanical Importance, *Int. J. Pure App. Biosci.*, 2017, **5**, 515–523.

91 Y. Liu, Y. Zhao and Y. Zhang, One-step green synthesized fluorescent carbon nanodots from bamboo leaves for copper(II) ion detection, *Sens. Actuators, B*, 2014, **196**, 647–652.

92 S. Ganguly, Medicinal Utility of Pomegranate Fruit in Regular Human Diet: A Brief Review, *Int. J. For. Hortic.*, 2017, **3**, 17–18.

93 F. Akhgari, K. Farhadi, N. Samadi and M. Akhgari, Detection of Silver Nanoparticles Using Green Synthesis of Fluorescent Nitrogen-Doped Carbon Dots, *Iran. J. Sci. Technol. Trans. A-Science*, 2020, **44**, 379–387.

94 B. Singh, P. Shankar, A. R. K. Mishra and H. Deupa, Potential of jackfruit seed as a functional ingredient: A Review, *Int. J. Agric. Food Sci.*, 2025, **7**, 283–289.

95 K. Raji, V. Ramanan and P. Ramamurthy, Facile and green synthesis of highly fluorescent nitrogen-doped carbon dots from jackfruit seeds and its applications towards the fluorimetric detection of Au^{3+} ions in aqueous medium and in *in vitro* multicolor cell imaging, *New J. Chem.*, 2019, **43**, 11710–11719.

96 S. Al-Assaf and G. O. Phillips, An Introduction to Gum Ghatti: Another Proteinaceous Gum, *Foods Food Ingredients J. Jpn.*, 2006, **211**(3), 275.

97 A. Sekar and R. Yadav, Green fabrication of zinc oxide supported carbon dots for visible light-responsive photocatalytic decolourization of Malachite Green dye: Optimization and kinetic studies, *Optik*, 2021, **242**, 167311.

98 K. Vigyan Kendra, I. Preeti Kumari, R. Kumar Maurya Scholar, V. Kumar, R. Kumar Verma, P. Kumari, R. Kumar Maurya, R. Verma and R. Kumar Singh, Medicinal properties of turmeric (Curcuma longa L.): A review, *Int. J. Chem. Stud.*, 2018, **6**, 1354–1357.

99 S. Ahmadian-Fard-Fini, M. Salavati-Niasari and H. Safardoust-Hojaghan, Hydrothermal green synthesis and photocatalytic activity of magnetic CoFe2O4–carbon quantum dots nanocomposite by turmeric precursor, *J. Mater. Sci.: Mater. Electron.*, 2017, **28**, 16205–16214.

100 P. Singh, P. P. Kannan, A. Dan, H. Vithalani, N. Singh, M. Dhanka, D. Bhatia and J. Saha, Comparative study of medicinal-plant-derived carbon nanoparticles: green synthesis, antioxidant behavior, and metal-ion sensing, *Nano Express*, 2026, **7**, 015013.

101 S. Zhu, Y. Song, X. Zhao, J. Shao, J. Zhang and B. Yang, The photoluminescence mechanism in carbon dots (graphene quantum dots, carbon nanodots, and polymer dots): current state and future perspective, *Nano Res.*, 2015, **8**, 355–381.

102 K. J. Mintz, Y. Zhou and R. M. Leblanc, Recent development of carbon quantum dots regarding their optical properties, photoluminescence mechanism, and core structure, *Nanoscale*, 2019, **11**, 4634–4652.

103 Y.-P. Sun, B. Zhou, Y. Lin, W. Wang, K. A. S. Fernando, P. Pathak, M. J. Meziani, B. A. Harruff, X. Wang, H. Wang, P. G. Luo, H. Yang, M. E. Kose, B. Chen, L. M. Veca and S.-Y. Xie, Quantum-Sized Carbon Dots for Bright and Colorful Photoluminescence, *J. Am. Chem. Soc.*, 2006, **128**, 7756–7757.

104 K. Muthamma, D. Sunil and P. Shetty, Carbon dots as emerging luminophores in security inks for anti-counterfeit applications - An up-to-date review, *Appl. Mater. Today*, 2021, **23**, 101050.

105 H. Li, X. He, Z. Kang, H. Huang, Y. Liu, J. Liu, S. Lian, C. H. A. Tsang, X. Yang and S. Lee, Water-Soluble Fluorescent Carbon Quantum Dots and Photocatalyst Design, *Angew. Chem., Int. Ed.*, 2010, **49**, 4430–4434.

106 M. A. Sk, A. Ananthanarayanan, L. Huang, K. H. Lim and P. Chen, Revealing the tunable photoluminescence properties of graphene quantum dots, *J. Mater. Chem. C*, 2014, **2**, 6954–6960.

107 S.-Y. Song, K.-K. Liu, Q. Cao, X. Mao, W.-B. Zhao, Y. Wang, Y.-C. Liang, J.-H. Zang, Q. Lou, L. Dong and C.-X. Shan, Ultraviolet phosphorescent carbon nanodots, *Light Sci. Appl.*, 2022, **11**, 146.

108 Y. Ding, X. Wang, M. Tang and H. Qiu, Tailored Fabrication of Carbon Dot Composites with Full-Color Ultralong Room-Temperature Phosphorescence for Multidimensional Encryption, *Adv. Sci.*, 2022, **9**(3), 2103833.

109 L. Sciortino, A. Sciortino, R. Popescu, R. Schneider, D. Gerthsen, S. Agnello, M. Cannas and F. Messina, Tailoring the Emission Color of Carbon Dots through Nitrogen-Induced Changes of Their Crystalline Structure, *J. Phys. Chem. C*, 2018, **122**, 19897–19903.

110 M. J. Krysmann, A. Kelarakis, P. Dallas and E. P. Giannelis, Formation Mechanism of Carbogenic Nanoparticles with Dual Photoluminescence Emission, *J. Am. Chem. Soc.*, 2012, **134**, 747–750.

111 S. Zhu, Y. Song, X. Zhao, J. Shao, J. Zhang and B. Yang, The photoluminescence mechanism in carbon dots (graphene quantum dots, carbon nanodots, and polymer dots): current state and future perspective, *Nano Res.*, 2015, **8**, 355–381.

112 L. Wang, S.-J. Zhu, H.-Y. Wang, S.-N. Qu, Y.-L. Zhang, J.-H. Zhang, Q.-D. Chen, H.-L. Xu, W. Han, B. Yang and H.-B. Sun, Common Origin of Green Luminescence in Carbon Nanodots and Graphene Quantum Dots, *ACS Nano*, 2014, **8**, 2541–2547.

113 L. Bao, Z. Zhang, Z. Tian, L. Zhang, C. Liu, Y. Lin, B. Qi and D. Pang, Electrochemical Tuning of Luminescent Carbon Nanodots: From Preparation to Luminescence Mechanism, *Adv. Mater.*, 2011, **23**, 5801–5806.

114 H. Qi, C. Liu, J. Jing, T. Jing, X. Zhang, J. Li, C. Luo, L. Qiu and Q. Li, Two kinds of biomass-derived carbon dots with one-step synthesis for Fe3+ and tetracyclines detection, *Dyes Pigm.*, 2022, **206**, 110555.

115 J. Schneider, C. J. Reckmeier, Y. Xiong, M. von Seckendorff, A. S. Susha, P. Kasák and A. L. Rogach, Molecular

Fluorescence in Citric Acid-Based Carbon Dots, *J. Phys. Chem. C*, 2017, **121**, 2014–2022.

116 K. Kalanidhi and P. Nagaraaj, Facile and Green synthesis of fluorescent N-doped carbon dots from betel leaves for sensitive detection of Picric acid and Iron ion, *J. Photochem. Photobiol., A*, 2021, **418**, 113369.

117 F. Zu, F. Yan, Z. Bai, J. Xu, Y. Wang, Y. Huang and X. Zhou, The quenching of the fluorescence of carbon dots: A review on mechanisms and applications, *Microchim. Acta*, 2017, **184**, 1899–1914.

118 *Principles of Fluorescence Spectroscopy*, ed. J. R. Lakowicz, Springer US, Boston, MA, 2006, pp. 27–61.

119 H. Liu, C. Xu, Y. Bai, L. Liu, D. Liao, J. Liang, L. Liu and H. Han, Interaction between fluorescein isothiocyanate and carbon dots: Inner filter effect and fluorescence resonance energy transfer, *Spectrochim. Acta, Part A*, 2017, **171**, 311–316.

120 X. Zhang, X. Liao, Y. Hou, B. Jia, L. Fu, M. Jia, L. Zhou, J. Lu and W. Kong, Recent advances in synthesis and modification of carbon dots for optical sensing of pesticides, *J. Hazard. Mater.*, 2022, **422**, 126881.

121 I. Kaur, V. Batra, N. K. R. Bogireddy, J. Baveja, Y. Kumar and V. Agarwal, Chemical- and green-precursor-derived carbon dots for photocatalytic degradation of dyes, *iScience*, 2024, **27**, 108920.

122 Y. Yu, Q. Zeng, S. Tao, C. Xia, C. Liu, P. Liu and B. Yang, Carbon Dots Based Photoinduced Reactions: Advances and Perspective, *Adv. Sci.*, 2023, **10**(12), 2207621.

123 A. Safaei, F. Giyahban and H. Ebrahimzadeh, Development of a ratiometric fluorescence sensor based on blue- and orange-emissive carbon dots for the determination of tartrazine in food products, *Food Chem.*, 2025, **477**, 143582.